This article has been accepted for publication in a future issue of this journal, but has not been fully edited. Content may change prior to final publication. Citation information: DOI 10.1109/TNSE.2017.2754944, IEEE Transactions on Network Science and Engineering

Weighted Bearing-Compass Dynamics: Edge and Leader Selection

Eric Schoof, Airlie Chapman, and Mehran Mesbahi

Abstract—This paper considers the design and effective interfaces of a distributed robotic formation running planar weighted bearing-compass dynamics. We present results which support methodologies to construct formation topologies using submodular optimization techniques. Further, a convex optimization framework is developed for the selection of edge weights which increase performance. We explore a method to select leader agents which can translate and scale the formation, and a corresponding controller that promotes the formation keeping its overall shape intact during manipulation. The results are supported with examples that illustrate the approach and their differing levels of performance.

Index Terms—Bearing rigidity, formation control, submodularity, network design, leader selection.

1 Introduction

The objective of formation control in multi-agent systems is to acquire and adapt the geometric configuration of agents, or formation shape, using distributed control protocols. The design of formation control algorithms can be broken into two main steps. The first is designing the distributed control protocol which will achieve a desired formation shape. The second step is manipulating the formation by adapting the formation protocol or augmenting the protocol with external signals. This paper builds on our previous work on bearing-compass dynamics [1] which provides a distributed dynamic model able to almost globally acquire a desired formation shape. The focus of this work is on developing theory and algorithms applicable to the bearing-dynamics dynamics to efficiently acquire and manipulate the formation shape. This is achieved through the selection of effective communication links and agents in the network - edges and leaders.

Bearing-compass dynamics fits under a broader class of dynamics referred to as distributed protocols. Distributed protocols are popular in the area of robotic formation control due to the fact that an individual agent needs only local information about its neighbors for operation [2], [3], [4], [5], [6], [7]. One of the most popular local information types is relative distance-based measurements [8], [9]. The examination of relative bearing-based measurements has become of interest in the last decade, with this current work fitting into this subclass [10], [11], [12], [13]. Both distance-based and bearing-based protocols rely on graph rigidity theory to guarantee that the protocols will converge to a unique formation shape based on the location of the relative measurements within the communication graph. The ability to reason about and design the placement of relative measurements within a network is one of the topics addressed in this paper.

$2n$. Similar to the selection under rank in §4.1 the minimum number of leader agents, namely two will be selected..

Designing topologies to optimize for a given metric has been addressed in the literature. These methods typically fit into two broad classes. The first class examines the continuous design of variables on the graph topology, e.g., through edge weights and input control weights. The second class is a combinatorial approach that examines node or edge selection problems. For example, Wan *et al.* maximized the largest eigenvalue of the graph Laplacian through the selection of edge weights [14]. Chapman *et al.* designed edge weights distributively and online to reject network-level disturbances [15]. Zelazo and Mesbahi leveraged convex optimization techniques to design edge weights for performance improvements under the $\mathcal{H}_2$ and $\mathcal{H}_\infty$ norms [16]. With the objective of maximizing the algebraic connectivity of the graph Laplacian, Ghosh and Boyd examined techniques to grow graphs with improved connectivity [17].

Augmenting distributed robotic algorithms with agents that are not following to the same control law has also been considered in recent years [18], [19]. These non-conforming agents are referred to as leaders, or anchors, while the others are named followers. The overall setup is commonly termed leader-follower dynamics. Zhao and Zelazo have considered the leader-follower setup for the bearing-compass dynamics as a method of controlling the translation and scale of the formation [13], [20]. Techniques from convex optimization and suboptimal greedy algorithms have been used to select influential access points into a network for leaders for the consensus dynamics, also referred to as the leader selection problem [21], [22], [23]. Examining leader selection for the bearing-compass dynamics is one of the problems addressed in this work.

Submodular optimization has emerged as a popular technique to solve the discrete topology design problem [24],

- *Eric Schoof is with the department of Electrical and Electronics Engineering, University of Melbourne, Australia. eschoof@unimelb.edu.au*
- *Airlie Chapman is with the department of Mechanical Engineering, University of Melbourne, Australia. airlie.chapman@unimelb.edu.au*
- *Mehran Mesbahi is with the William E. Boeing department of Aeronautics and Astronautics, University of Washington, USA. mesbahi@uw.edu.*

The research of the authors has been supported by ARO grant W911NF-13-1-0340 and AFOSR grant FA9550-16-1-0022.

This article has been accepted for publication in a future issue of this journal, but has not been fully edited. Content may change prior to final publication. Citation information: DOI 10.1109/TNSE.2017.2754944, IEEE Transactions on Network Science and Engineering

[25], [26], [27]. An attraction of this theory is that greedy selection heuristics may be employed to achieve provably near-optimal solutions. The current work will rely heavily on this framework to design well-performing graphs under bearing rigidity performance measures. A related work by Shames and Summers examined a similar approach to build distance rigid formations and select influential leader locations within a network using submodular optimality theory [28].

The contribution of this paper is two-fold. First, we extend the bearing-compass dynamics [1], [13] to allow different weights on the agent interaction topology and include the addition of fixed anchors. Second, we use the field of submodular optimization to build and manipulate formations via edge and node selection, respectively. This provides provably near-optimal selection performance that would be computationally infeasible to perform optimally. We show how several possible submodular metrics perform under edge and node selection. We also use convex optimization to select edge weights that improve the convergence of formation acquisition and manipulation protocols without increasing the required control authority for any individual agent in the formation.

We begin by introducing background concepts and notation in §2. In §3, we extend our previous work [1], [6] and the work of others [11], [12], [13] by examining properties of a weighted version of the bearing-compass dynamics. We proceed in §4 to discuss a process by which one can define a formation for favorable performance under the dynamics. Next, in §5, we explore how we can move or scale a formation running the weighted bearing-compass dynamics so it can be placed in a desired orientation through leader selection. A state-dependent weighting scheme is presented which allows the formation to more easily retain its shape while it is being manipulated. Concluding remarks and notes on future directions are provided in §6.

2 Background

In this section, a brief background is provided on the notation, dynamics and definitions that are used in this paper.

Given a matrix $A \in \mathbb{R}^{m\times n}$, the notation $[A]_{ij}$ is used to represent the element of A in row $i \in 1,\dots,m$ and column $j \in 1,\dots,n$. The eigenvalues of a matrix $A \in \mathbb{R}^{n\times n}$ are notated as $\lambda_i(A)$ and ordered such that $\mathrm{Re}\lambda_1(A) \leq \mathrm{Re}\lambda_2(A) \leq \cdots \leq \mathrm{Re}\lambda_n(A)$. The notation $A \succ 0$ and $A \succeq 0$ designates the matrix A as being *positive definite* and *positive semi-definite*, respectively. We use the notation $\mathbf{0}$ and $\mathbf{1}$ to refer to the vectors of all zeros and all ones, respectively, with the dimension inferred from the context. The 2-norm of a vector $\mathbf{v}$ is denoted $\|\mathbf{v}\|$. The normalized vector of $\mathbf{v}$ is denoted $\hat{\mathbf{v}} = \mathbf{v}/\|\mathbf{v}\|$. Given a vector $\mathbf{v} \in \mathbb{R}^2$, the *perpendicular* of $\mathbf{v} = \begin{bmatrix} v_1 & v_2 \end{bmatrix}^T$ is $\mathbf{v}^\perp = \begin{bmatrix} -v_2 & v_1 \end{bmatrix}^T$.We represent block diagonal matrices with a repeated structure as $\mathcal{D}_i(A_i)$, where A_i appears as the ith block diagonal of $\mathcal{D}$. Given vectors $\mathbf{a},\mathbf{b} \in \mathbb{R}^2$, the *projection* of $\mathbf{a}$ onto $\mathbf{b}$ is defined as $\mathrm{Proj}_{\mathbf{b}}\mathbf{a} = (\mathbf{a}^T\mathbf{b}/\|\mathbf{a}\|\|\mathbf{b}\|)\mathbf{b}$ implying that $\mathbf{a} - \mathrm{Proj}_{\mathbf{b}}\mathbf{a} = \mathrm{Proj}_{\mathbf{b}^\perp}\mathbf{a}$.

We denote *undirected weighted graphs* as $\mathcal{G} = (V,E,\mathbf{w})$, where V is the set of *nodes* $i \in V$ with cardinality $|V| = n$ and E is the set of *edges* $\{i,j\} \in E$, with $i,j \in V$ and cardinality $|E| = m$. The *incidence matrix* $H \in \mathbb{R}^{m\times n}$ encodes the edge set E such that for edge k representing edge $\{i,j\} \in E$, $[H]_{ki} = -1$ and $[H]_{kj} = 1$, and $i < j$. If edge $\{i,j\} \in E$ is the kth row in the incidence matrix H, then the relative state between agents i and j can be written $\mathbf{r}_j - \mathbf{r}_i = \mathbf{r}_{ij} = \mathbf{r}_{\bar{k}}$, which disambiguates the state of node k and the relative state of the nodes incident on edge $\bar{k}$. We then have the relation that $\widetilde{H}\mathbf{r} = \begin{bmatrix} \mathbf{r}_{\bar{1}}^T & \mathbf{r}_{\bar{2}}^T & \cdots & \mathbf{r}_{\bar{m}}^T \end{bmatrix}^T$, where $\mathbf{r} \in \mathbb{R}^{2n}$, $\widetilde{H} = (H \otimes I_2)$, and $\otimes$ denotes the Kronecker product. The vector $\mathbf{w} \in \mathbb{R}^m$ is the weight vector with elements $w_{\bar{k}}$ for each edge $\bar{k} \in E$. If $\mathbf{w}$ is omitted, we assume that $\mathbf{w} = \mathbf{1}$ and write $\mathcal{G} = (V,E)$. We define the set of neighbors of agent i as $j \in \mathcal{N}(i)$ if $\{i,j\} \in E$, where $\mathcal{N}(i)$ is called the *neighborhood* of i.

2.1 Modular and Submodular Functions

We denote functions of the form $f(S) : 2^n \to \mathbb{R}$, where $S \subseteq \mathcal{S}$ and $|\mathcal{S}| = n$, as *set functions*. The *empty set* is denoted $\emptyset$. These functions can have many properties that we can exploit, some of which are reviewed next.

Definition 1. A set function $f(S) : 2^n \to \mathbb{R}$ is *modular* if for all subsets $S \subseteq \mathcal{S}$ it can be expressed as

$$f(S) = w(\emptyset) + \sum_{s\in S} w(s),$$

for some weight function $w : s \in \mathcal{S} \to \mathbb{R}$.

Definition 2. A set function $f(S) : 2^n \to \mathbb{R}$ is *monotone increasing* if, for all subsets $A \subseteq B \subseteq \mathcal{S}$ it holds that $f(A) \leq f(B)$.

Definition 3. [24, Def. 2.1] A set function $f(S) : 2^n \to \mathbb{R}$ is *submodular* if, for all subsets $A \subseteq B \subseteq \mathcal{S}$ and $s \notin B$, then

$$f(A \cup \{s\}) - f(A) \geq f(B \cup \{s\}) - f(B). \tag{1}$$

Modular functions can be considered a special case of submodular functions where equality holds in (1). The intuition behind Def. 3 is that adding an element to a smaller set gives a greater gain than adding the same element to a larger set, sometimes called "diminishing returns". Submodular functions bear similarities to convex functions [25]. This connection can be used to provide guarantees on greedy algorithms optimizing over submodular functions which is explored in Thm 5 below.

Proposition 4. *[24, Prop. 2.7] A positive linear combination of submodular functions is submodular.*

Theorem 5. *[24, Thm 4.3] Consider the problem of selecting K elements from a set $\mathcal{S}$ which optimizes the value of a monotonically increasing submodular cost function $f(S)$ for $S \in \mathcal{S}$ and $|S| = K$. If we make a greedy selection of R elements at each iteration, then the value of our greedy selection $f(S)$ will satisfy*

$$\frac{f(S) - f(\emptyset)}{f(S^*) - f(\emptyset)} \geq 1 - \left(\frac{q-\lambda}{q}\right)\left(\frac{q-1}{q}\right)^{q-1}, \tag{2}$$

where S^* is the globally optimal selection, $K = qR - p$ for some $q \in \mathbb{Z}^+$, p an integer in the range $0 \leq p \leq R-1$, and $\lambda = \frac{R-p}{R}$.

This article has been accepted for publication in a future issue of this journal, but has not been fully edited. Content may change prior to final publication. Citation information: DOI 10.1109/TNSE.2017.2754944, IEEE Transactions on Network Science and Engineering

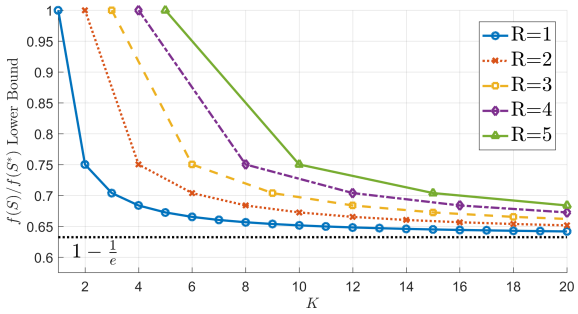

Figure 1: Optimality bound when performing a greedy selection of K elements over a submodular cost function, for different batch sizes R, assuming $f(\emptyset) = 0$.

When K is an integer multiple of R, the bound in Eq. (2) becomes tight. For the case when $R = 1$, Eq. (2) becomes

$$\frac{f(S) - f(\emptyset)}{f(S^*) - f(\emptyset)} \geq 1 - \left(\frac{K-1}{K}\right)^K \geq 1 - \frac{1}{e} \approx 63\%. \quad (3)$$

The last approximation is obtained in the limit as $K \to \infty$.

A consequence of Thm 5 is that picking K items from a set one at a time using a greedy submodular heuristic, i.e., adding an element to a set which maximizes the heuristic at each step, will return a solution whose value is within approximately 37% of the optimal solution. Different bounds can be obtained by varying K and R, as demonstrated in Fig. 1.

2.2 Bearing Measurements on a Graph

In this paper, we use the term "node" to describe a particular element of V. There is also a more loosely termed "agent" which refers to something (usually a vehicle) that can communicate or act *through* the edges of E, and can have its own state. We define the agent positions in 2-D space at time t by the vector $\mathbf{r}(t) = [\ \mathbf{r}_1^T(t) \quad \mathbf{r}_2^T(t) \quad \dots \quad \mathbf{r}_n^T(t)\ ]^T$, where $\mathbf{r}_i(t) = [\ r_{ix}(t) \quad r_{iy}(t)\ ]^T$. Core to this paper, is understanding agents formation shape when a family of bearing constraints are placed on pairs of agents. To this end, we use the term *formation*, denoted with $\mathbf{f} \in \mathbb{R}^{2n}$, to represent a desired state for a collection of agents. Franchi and Giordano [12] explored the notion of coupling of a formation with a graph, using the pairwise bearing measurement set

$$\Theta(\mathcal{G}, \mathbf{f}) = \left\{\hat{\mathbf{f}}_{ij} \ : \ \{i,j\} \in E\right\}. \quad (4)$$

We will take an excursion from Franchi and Giordano terminology and refer to this as a *framework*. The collection of agent formations $\mathbf{r}$ which are *bearing equivalent*, or just equivalent, to a given framework Θ is denoted by

$$\chi(\Theta) = \left\{\mathbf{r} \ : \ \hat{\mathbf{r}}_{ij}^T \hat{\mathbf{f}}_{ij}^{\perp} = 0, \forall \hat{\mathbf{f}}_{ij} \in \Theta\right\}. \quad (5)$$

The set of bearing equivalent formations represents those agent locations that conform to the bearing constraints in Θ. A formation $\mathbf{f}$ and $\mathbf{g}$ are *similar* if $\mathbf{g}$ is a translated and/or scaled version of $\mathbf{f}$. If all equivalent formations are similar then the framework is termed *parallel rigid* or *bearing rigid*. Algebraic conditions that guarantee bearing rigidity based on the notion of infinitesimal bearing rigidity will be explored in §3. In order to more easily classify similar formations, we introduce the notion of centroid and scale of a formation [1], [13]. Given a set of agents at positions $\mathbf{r} \in \mathbb{R}^{2n}$, the *centroid* of the agents is defined as

$$C(\mathbf{r}) = \frac{1}{n} \sum_{i \in V} \mathbf{r}_i. \quad (6)$$

The *scale* of the agents on the other hand is defined as

$$S(\mathbf{r}) = \sqrt{\frac{1}{n} \sum_{i \in V} \|\mathbf{q}_i\|^2}, \quad (7)$$

where $\mathbf{q}_i := \mathbf{r}_i - C(\mathbf{r})$. Given a formation $\mathbf{f} \in \mathbb{R}^{2n}$, the *unitless formation* $\tilde{\mathbf{f}}$ is defined as

$$\tilde{\mathbf{f}} = \left[\mathbf{f} - (I_n \otimes C(\mathbf{f}))\, \mathbf{1}_n\right] S(\mathbf{f})^{-1}, \quad (8)$$

with properties $C(\tilde{\mathbf{f}}) = \mathbf{0}$, $S(\tilde{\mathbf{f}}) = 1$, and $\left\|\tilde{\mathbf{f}}\right\| = \sqrt{n}$. We note a unitless formation $\tilde{\mathbf{f}}$ is similar to $\mathbf{f}$.

The unique pair of similar formations to formation $\mathbf{f}$ which share the same scale and centroid as $\mathbf{r}$ is defined as

$$\begin{aligned} \xi_{\pm}(\mathbf{f}, \boldsymbol{r}) &= \pm \tilde{\mathbf{f}} S(\mathbf{r}) + (I_n \otimes C(\mathbf{r}))\, \mathbf{1} \quad (9) \\ &= \{\xi_+(\mathbf{f}, \boldsymbol{r}), \xi_-(\mathbf{f}, \boldsymbol{r})\}, \end{aligned}$$

where $\xi_+(\mathbf{f}, \boldsymbol{r})$ and $\xi_-(\mathbf{f}, \boldsymbol{r})$ denote the positively and negatively scaled formations, respectively.

3 Weighted Bearing-Compass Dynamics

In this paper, we extend the analysis of our previously introduced bearing-compass particle dynamics [1] with a weighting term on each edge as

$$\dot{\mathbf{r}}_i = \mathbf{u}_i(\Theta) + \tilde{\mathbf{u}}_i \quad (10a)$$

$$\mathbf{u}_i(\Theta) = \sum_{j \in \mathcal{N}(i)} w_{ij} (\hat{\mathbf{r}}_{ij}^T \hat{\mathbf{f}}_{ij}^{\perp}) \hat{\mathbf{r}}_{ij}^{\perp} := \sum_{i \in \mathcal{N}(i)} \mathbf{u}_{(ij)}, \quad (10b)$$

where $\Theta = (\mathcal{G}, \mathbf{f})$, $\mathcal{G} = (V, E, \mathbf{w})$. Here, we use the notation $\mathbf{b}_{(ij)}$ to represent the component of $\mathbf{b}_i$ due to j. We note the notation $\mathbf{b}_{(ij)}$ is distinct from $\mathbf{b}_{ij}$ and that $\mathbf{b}_{(\bar{k})}$ can be used in place of $\mathbf{b}_{(ij)}$ when edge indexing is preferable. If $\tilde{\mathbf{u}}_i = \mathbf{0}$ for all $i \in V$, then we say the dynamics is *unforced*. Otherwise, we say the dynamics is *forced*.

The dynamics is referred to as bearing-compass as it can be implemented with only relative bearing information to neighboring agents and access to a compass to localize the measurements in a frame. The former can be achieved via an on-board low-fidelity camera [7] where distance measurements can be unreliable compared to bearing measurements. Agents with $\tilde{\mathbf{u}}_i \neq 0$ are referred to as *leader* agents, as through the networked dynamics, the non-leader agents follow the leaders.

As we proceed through this section, we will look at various features of the bearing-compass dynamics. To this end, the following proposition is a useful tool which will be used throughout this paper to simplify our proofs.

Proposition 6. *If $\mathbf{b}_{(ij)} = -\mathbf{b}_{(ji)}$, enumeration over nodes and neighborhoods is equivalent to enumeration over edges with*

$$\sum_{i \in V} \mathbf{a}_i^T \sum_{j \in \mathcal{N}(i)} \mathbf{b}_{(ij)} = -\sum_{\bar{k} \in E} \mathbf{a}_{\bar{k}}^T \mathbf{b}_{(\bar{k})}.$$

This article has been accepted for publication in a future issue of this journal, but has not been fully edited. Content may change prior to final publication. Citation information: DOI 10.1109/TNSE.2017.2754944, IEEE Transactions on Network Science and Engineering

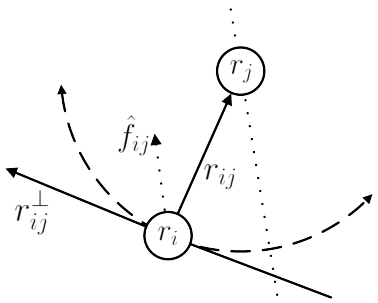

Figure 2: Vector definitions for dynamics (10).

Proof: Noting that LHS represents an enumeration of every edge twice, once representing $\mathbf{a}_i^T\mathbf{b}_{(ij)}$ and once representing $\mathbf{a}_j^T\mathbf{b}_{(ji)}$, the result follows. □

The unforced bearing-compass dynamics exhibits properties such as invariance of the formation centroid and scale, which make it attractive for maintaining stable formations. The forced dynamics is then able to directly manipulate the centroid and scale. The following proposition formerly presents these properties.

Proposition 7. *Under the weighted dynamics (10), the formation centroid and scale evolve as*

$$\begin{aligned}\frac{\partial C(\mathbf{r})}{\partial t} &= \frac{1}{n}\sum_{i\in V}\tilde{\mathbf{u}}_i \\ \frac{\partial S(\mathbf{r})}{\partial t} &= \frac{2}{nS(\mathbf{r})}\sum_{i\in V}\mathbf{q}_i^T(\tilde{\mathbf{u}}_i - \frac{1}{n}\sum_{j\in V}\tilde{\mathbf{u}}_j).\end{aligned}$$

Additionally, if $\tilde{\mathbf{u}}_i = \mathbf{0}$ for all $i \in V$, then $\partial C(\mathbf{r})/\partial t = \mathbf{0}$ and $\partial S(\mathbf{r})/\partial t = 0$, and the centroid and scale are said to be invariant under the unforced dynamics.

Proof: Differentiating Eq. (6), we have

$$\begin{aligned}\frac{\partial C(\mathbf{r})}{\partial t} &= \frac{1}{n}\sum_{i\in V}\dot{\mathbf{r}} = \frac{1}{n}\sum_{i\in V}(\mathbf{u}_i + \tilde{\mathbf{u}}_i) \\ &= \frac{1}{n}\sum_{\{i,j\}\in E}\left(\mathbf{u}_{(ij)} + \mathbf{u}_{(ji)}\right) + \frac{1}{n}\sum_{i\in V}\tilde{\mathbf{u}}_i \\ &= \frac{1}{n}\sum_{i\in V}\tilde{\mathbf{u}}_i.\end{aligned}$$

Similarly, if we differentiate Eq. (7), we have

$$\begin{aligned}\frac{\partial S(\mathbf{r})}{\partial t} &= \frac{\partial}{\partial t}\sqrt{\frac{1}{n}\sum_{i\in V}\mathbf{q}_i^T\mathbf{q}_i} \\ &= \frac{1}{\sqrt{n\sum_{i\in V}\mathbf{q}_i^T\mathbf{q}_i}}\frac{\partial}{\partial t}\mathbf{q}_i^T\mathbf{q}_i \\ &= \frac{2}{nS(\mathbf{r})}\sum_{i\in V}\mathbf{q}_i^T(\tilde{\mathbf{u}}_i - \frac{1}{n}\sum_{j\in V}\tilde{\mathbf{u}}_j),\end{aligned}$$

where the final equality comes from a similar proof in [1]. □

In order to examine the dynamics (10) it is helpful to have a machinery to encode the bearing information embedded within the dynamics. The bearing rigidity matrix has this function and can be constructed from the formation $\mathbf{f}$ and the underlying graph $\mathcal{G}$.

Definition 8. The *bearing rigidity matrix* is denoted $\mathcal{R}(\Theta)$, where $\Theta(\mathcal{G}, \mathbf{f})$ is the framework, is defined as

$$\mathcal{R}(\Theta) = \frac{\partial\hat{\mathbf{g}}}{\partial\mathbf{f}}, \tag{11}$$

where $\mathbf{g} = \widetilde{H}\mathbf{f}$, and $\hat{\mathbf{g}} = \begin{bmatrix}\hat{\mathbf{f}}_{\bar{1}}^T & \hat{\mathbf{f}}_{\bar{2}}^T & \cdots & \hat{\mathbf{f}}_{\bar{m}}^T\end{bmatrix}^T$. An alternative expression for (11) is[1]

$$\begin{aligned}\mathcal{R}(\Theta) &= \mathcal{D}_{\bar{k}}\left[\frac{1}{\|\mathbf{f}_{\bar{k}}\|}I_d\right]\mathcal{D}_{\bar{k}}[P_{\bar{k}}]\,\tilde{H} \\ &:= \mathcal{D}_{\bar{k}}\left[\frac{1}{\|\mathbf{f}_{\bar{k}}\|}I_d\right]\widetilde{\mathcal{R}}(\Theta),\end{aligned}$$

where $P_{\bar{k}} := I_2 - \hat{\mathbf{f}}_{\bar{k}}\hat{\mathbf{f}}_{\bar{k}}^T$ is a projection onto the orthogonal complement of $\mathbf{f}_{\bar{k}}$, and $\widetilde{\mathcal{R}}(\Theta)$ is called the *unit rigidity matrix*.

The rigidity matrix exhibits the property that $\mathbf{r} \in \chi(\Theta)$ if and only if $\mathcal{R}(\Theta)\boldsymbol{r} = 0$, or equivalently $\widetilde{\mathcal{R}}(\Theta)\mathbf{r} = 0$.

Theorem 9. *Under the unforced dynamics (10), $\mathbf{r}(t)$ will asymptotically converge to $\chi(\Theta)$.*

Proof: Without loss of generality, let the centroid of $\mathbf{r}(0)$ be the origin. Let $\mathbf{f} = \xi_+(\mathbf{f}, \boldsymbol{r}(0))$. Consequently, $\|\mathbf{r}(0)\| = \|\mathbf{f}\|$ and $C(\mathbf{f}) = 0$. Applying the change of variable $\mathbf{z} = \mathbf{r} - \mathbf{f}$, where $\mathbf{r}_{ij} = \mathbf{z}_{ij} + \mathbf{f}_{ij}$, then for each $i \in V$,

$$\begin{aligned}\dot{\mathbf{z}}_i &= \sum_{j\in\mathcal{N}(i)} w_{ij}\hat{\mathbf{r}}_{ij}^T\hat{\mathbf{f}}_{ij}^{\perp}\hat{\mathbf{r}}_{ij}^{\perp} \\ &= \sum_{j\in\mathcal{N}(i)}\frac{w_{ij}}{\|\mathbf{z}_{ij}+\mathbf{f}_{ij}\|^2}(\mathbf{z}_{ij}+\mathbf{f}_{ij})^T\hat{\mathbf{f}}_{ij}^{\perp}(\mathbf{z}_{ij}+\mathbf{f}_{ij})^{\perp} \\ &= \sum_{j\in\mathcal{N}(i)}\frac{w_{ij}\mathbf{z}_{ij}^T\hat{\mathbf{f}}_{ij}^{\perp}}{\|\mathbf{z}_{ij}+\mathbf{f}_{ij}\|^2}(\mathbf{z}_{ij}+\mathbf{f}_{ij})^{\perp} \\ &:= \sum_{j\in\mathcal{N}(i)}\mathbf{g}_{(ij)}(\mathbf{z},\mathbf{f}).\end{aligned} \tag{12}$$

Consider the Lyapunov function $V(\mathbf{z}) = \frac{1}{2}\mathbf{z}^T\mathbf{z}$, we can expand its time derivative using Eq. (12) and apply Prop. 6 as

$$\begin{aligned}\dot{V}(\mathbf{z}) &= \sum_{i\in V}\mathbf{z}_i^T\sum_{j\in\mathcal{N}(i)}\mathbf{g}_{(ij)}(\mathbf{z},\mathbf{f}) \\ &= -\sum_{\bar{k}\in E}\mathbf{z}_{\bar{k}}^T\mathbf{g}_{(\bar{k})} \\ &= -\sum_{\bar{k}\in E}\frac{w_{\bar{k}}\mathbf{z}_{\bar{k}}^T\mathbf{z}_{\bar{k}}^T\hat{\mathbf{f}}_{\bar{k}}^{\perp}}{\|\mathbf{z}_{\bar{k}}+\mathbf{f}_{\bar{k}}\|^2}(\mathbf{z}_{\bar{k}}+\mathbf{f}_{\bar{k}})^{\perp} \\ &= -\sum_{\bar{k}\in E}\frac{w_{\bar{k}}\mathbf{z}_{\bar{k}}^T\hat{\mathbf{f}}_{\bar{k}}^{\perp}}{\|\mathbf{z}_{\bar{k}}+\mathbf{f}_{\bar{k}}\|^2}\left(\mathbf{z}_{\bar{k}}^T\mathbf{z}_{\bar{k}}^{\perp}+\mathbf{z}_{\bar{k}}^T\mathbf{f}_{\bar{k}}^{\perp}\right) \\ &= -\sum_{\bar{k}\in E}\frac{w_{\bar{k}}\left(\mathbf{z}_{\bar{k}}^T\mathbf{f}_{\bar{k}}^{\perp}\right)^2}{\|\mathbf{f}_{\bar{k}}\|\,\|\mathbf{z}_{\bar{k}}+\mathbf{f}_{\bar{k}}\|^2}.\end{aligned} \tag{13}$$

As $\dot{V}(\mathbf{z}) \le 0$ and $\dot{V}(\mathbf{z}) = 0$ if and only if $\mathbf{z} \in \chi(\Theta)$, it follows that $\mathbf{r} \in \chi(\Theta)$ and $\mathbf{r}(t)$ converges to $\chi(\Theta)$, establishing asymptotic stability by La Salle's theorem [29]. □

1. It is assumed throughout that no two agents are coincident within a formation, and so $\|\mathbf{f}_{\bar{k}}\| \neq 0$.

This article has been accepted for publication in a future issue of this journal, but has not been fully edited. Content may change prior to final publication. Citation information: DOI 10.1109/TNSE.2017.2754944, IEEE Transactions on Network Science and Engineering

Asymptotic convergence to $\chi(\Theta)$ can be further strengthened to exponential stability. This is explored in the following theorem.

Theorem 10. *Under the unforced dynamics (10), the Lyapunov function* $V = \frac{1}{2}(\mathbf{r}-\mathbf{f})^T(\mathbf{r}-\mathbf{f}) := \frac{1}{2}\mathbf{z}^T\mathbf{z}$ *satisfies*

$$\dot{V} \leq S(\mathbf{f})^{-1}\mathbf{z}^T\widetilde{\mathcal{R}}^T\mathcal{D}_{\bar{k}}\left[m_{\bar{k}}^2 I_2\right]\widetilde{\mathcal{R}}\mathbf{z} := -S(\mathbf{f})^{-1}\mathbf{z}^T Q\mathbf{z},$$

where $\mathbf{f} = \xi_+(\mathbf{f}, \boldsymbol{r}(0))$, *and we define the term* $m_{\bar{k}}^2(\mathbf{r}_0) := w_{\bar{k}}\left\|\tilde{\mathbf{f}}_{\bar{k}}\right\| / \left(S(\mathbf{f})^{-1}\|\mathbf{z}_0\| + \left\|\tilde{\mathbf{f}}_{\bar{k}}\right\|\right)^2$. *Consequently,* $\mathbf{r}(t)$ *will globally exponentially converge to* $\chi(\Theta)$.

Proof: If we expand Eq. (13), we have

$$\begin{aligned}
\dot{V}(\mathbf{z}) &= -\sum_{\bar{k}\in E}\frac{w_{\bar{k}}\left((\mathbf{r}_{\bar{k}}-\mathbf{f}_{\bar{k}})^T\mathbf{f}_{\bar{k}}^{\perp}\right)^2}{\|\mathbf{f}_{\bar{k}}\|\|\mathbf{r}_{\bar{k}}-\mathbf{f}_{\bar{k}}+\mathbf{f}_{\bar{k}}\|^2} \\
&= -\sum_{\bar{k}\in E}\frac{w_{\bar{k}}\left(\mathbf{r}_{\bar{k}}^T\mathbf{f}_{\bar{k}}^{\perp}\right)^2}{\|\mathbf{f}_{\bar{k}}\|\|\mathbf{r}_{\bar{k}}\|^2} \\
&= -\sum_{\bar{k}\in E}\frac{w_{\bar{k}}\|\mathbf{f}_{\bar{k}}\|}{\|\mathbf{r}_{\bar{k}}\|^2}\mathbf{r}_{\bar{k}}^T\left(\hat{\mathbf{f}}_{\bar{k}}^{\perp T}\mathbf{r}_{\bar{k}}\right)\hat{\mathbf{f}}_{\bar{k}}^{\perp}.
\end{aligned}$$

We now apply the relationship

$$(\hat{\mathbf{f}}_{\bar{k}}^{\perp T}\mathbf{r}_{\bar{k}})\hat{\mathbf{f}}_{\bar{k}}^{\perp} = \mathrm{Proj}_{\hat{\mathbf{f}}_{\bar{k}}^{\perp}}\mathbf{r}_{\bar{k}} = \mathbf{r}_{\bar{k}} - \mathrm{Proj}_{\hat{\mathbf{f}}_{\bar{k}}}\mathbf{r}_{\bar{k}} = P_{\bar{k}}\mathbf{r}_{\bar{k}}$$

to see that

$$\begin{aligned}
\dot{V}(\mathbf{z}) &= -\sum_{\bar{k}\in E}\mathbf{r}_{\bar{k}}^T w_{\bar{k}}\frac{\|\mathbf{f}_{\bar{k}}\|}{\|\mathbf{r}_{\bar{k}}\|^2}P_{\bar{k}}\mathbf{r}_{\bar{k}} \\
&= -\mathbf{r}^T\widetilde{H}^T\mathcal{D}_{\bar{k}}\left[w_{\bar{k}}\frac{\|\mathbf{f}_{\bar{k}}\|}{\|\mathbf{r}_{\bar{k}}\|^2}P_{\bar{k}}\right]\widetilde{H}\mathbf{r}. \qquad (14)
\end{aligned}$$

Now, we observe that

$$\mathcal{D}_{\bar{k}}\left[w_{\bar{k}}\frac{\|\mathbf{f}_{\bar{k}}\|}{\|\mathbf{r}_{\bar{k}}\|^2}P_{\bar{k}}\right]\widetilde{H}\mathbf{f} = \mathbf{0} \qquad (15)$$

as $P_{\bar{k}}\mathbf{f}_{\bar{k}} = \mathbf{0}$ due to $P_{\bar{k}}$ being a projection onto the orthogonal complement of $\mathbf{f}_{\bar{k}}$. Thus, we can add Eq. (15) into Eq. (14) as

$$\begin{aligned}
\dot{V}(\mathbf{z}) &= -(\mathbf{r}-\mathbf{f})^T\widetilde{H}^T\mathcal{D}_{\bar{k}}\left[w_{\bar{k}}\frac{\|\mathbf{f}_{\bar{k}}\|}{\|\mathbf{r}_{\bar{k}}\|^2}P_{\bar{k}}\right]\widetilde{H}(\mathbf{r}-\mathbf{f}) \\
&= -\mathbf{z}^T\widetilde{H}^T\mathcal{D}_{\bar{k}}\left[w_{\bar{k}}\frac{\|\mathbf{f}_{\bar{k}}\|}{\|\mathbf{r}_{\bar{k}}\|^2}P_{\bar{k}}\right]\widetilde{H}\mathbf{z}.
\end{aligned}$$

Similarly, we can also introduce an additional $\mathcal{D}_{\bar{k}}[P_{\bar{k}}]$ term, using the fact that $P_{\bar{k}}$ is a projection matrix and so $P_{\bar{k}}^2 = P_{\bar{k}}$. Thus,

$$\dot{V}(\mathbf{z}) = -\mathbf{z}^T\widetilde{H}^T\mathcal{D}_{\bar{k}}[P_{\bar{k}}]^T\mathcal{D}_{\bar{k}}\left[\frac{w_{\bar{k}}\|\mathbf{f}_{\bar{k}}\|}{\|\mathbf{r}_{\bar{k}}\|^2}I_2\right]\mathcal{D}_{\bar{k}}[P_{\bar{k}}]\widetilde{H}\mathbf{z}.$$

However,

$$\frac{\|\mathbf{f}_{\bar{k}}\|}{\|\mathbf{r}_{\bar{k}}\|^2} = \frac{\|\mathbf{f}_{\bar{k}}\|}{\|\mathbf{z}_{\bar{k}}+\mathbf{f}_{\bar{k}}\|^2} \geq \frac{\|\mathbf{f}_{\bar{k}}\|}{(\|\mathbf{z}_{\bar{k}}\|+\|\mathbf{f}_{\bar{k}}\|)^2}.$$

Applying Thm 9, $\|\mathbf{z}_{\bar{k}}\| \leq \|\mathbf{z}\| \leq \|\mathbf{z}_0\|$. Thus, we can write

$$\begin{aligned}
\frac{w_{\bar{k}}\|\mathbf{f}_{\bar{k}}\|}{\|\mathbf{r}_{\bar{k}}\|^2} &\geq \frac{w_{\bar{k}}S(\mathbf{f})\left\|\tilde{\mathbf{f}}_{\bar{k}}\right\|}{\left(\|\mathbf{z}_0\|+S(\mathbf{f})\left\|\tilde{\mathbf{f}}_{\bar{k}}\right\|\right)^2} \\
&= S(\mathbf{f})^{-1}\frac{w_{\bar{k}}\left\|\tilde{\mathbf{f}}_{\bar{k}}\right\|}{\left(S(\mathbf{f})^{-1}\|\mathbf{z}_0\|+\left\|\tilde{\mathbf{f}}_{\bar{k}}\right\|\right)^2} := S(\mathbf{f})^{-1}m_{\bar{k}}^2.
\end{aligned}$$

From the definition of $m_{\bar{k}}^2$ and the unit rigidity matrix $\widetilde{\mathcal{R}}$ then

$$\dot{V} \leq -S(\mathbf{f})^{-1}\mathbf{z}^T\widetilde{\mathcal{R}}^T\mathcal{D}_{\bar{k}}\left[m_{\bar{k}}^2 I_2\right]\widetilde{\mathcal{R}}\mathbf{z}.$$

The worst case initial error is $\|\mathbf{z}_0\| \leq \|-2\mathbf{f}\| = 2\sqrt{n}S(\mathbf{f})$, which follows from the fact that the trajectory of the error $\mathbf{z}$ under the dynamics (10) travels along a sphere of radius $\|\mathbf{f}\|$ [1], [13]. Noting that $m_{\bar{k}}^2 \geq w_{\bar{k}}\left\|\tilde{\mathbf{f}}_{\bar{k}}\right\| / \left(2\sqrt{n}+\left\|\tilde{\mathbf{f}}_{\bar{k}}\right\|\right)^2$, let $\beta = \min_{\bar{k}} m_{\bar{k}} > 0$, then

$$\dot{V}(\mathbf{z}) \leq -\beta S(\mathbf{f})^{-1}\mathbf{z}^T\widetilde{\mathcal{R}}^T\widetilde{\mathcal{R}}\mathbf{z}.$$

Isolating the components of $\mathbf{z}$ that are orthogonal to the nullspace of $\widetilde{\mathcal{R}}$, denoted $\mathbf{z}_{\perp}$, then

$$\begin{aligned}
\dot{V}(\mathbf{z}_{\perp}) &\leq -\beta S(\mathbf{f})^{-1}\lambda_q\left(\widetilde{\mathcal{R}}^T\widetilde{\mathcal{R}}\right)\mathbf{z}_{\perp}^T\mathbf{z}_{\perp} \\
&= -\beta S(\mathbf{f})^{-1}\lambda_q\left(\widetilde{\mathcal{R}}^T\widetilde{\mathcal{R}}\right)V(\mathbf{z}_{\perp}),
\end{aligned}$$

where $\lambda_q\left(\widetilde{\mathcal{R}}^T\widetilde{\mathcal{R}}\right) > 0$ is the smallest non-zero eigenvalue of $\widetilde{\mathcal{R}}^T\widetilde{\mathcal{R}}$. Hence the dynamics will converge exponentially to the nullspace of $\widetilde{\mathcal{R}}$, or equivalently, to $\chi(\Theta)$ by La Salle's theorem [29]. □

Theorem 10 describes convergence to the set $\chi(\Theta)$. To guarantee that the steady state formation is parallel to $\mathbf{f}$ then the framework must be bearing rigid. With this is mind, Zhao and Zelazo [13] examined the effect of a small change in agent positions $\triangle\mathbf{r} \in \mathbb{R}^{2n}$ with respect to the bearing measurements, where if $\mathcal{R}(\Theta)\triangle\mathbf{r} = \mathbf{0}$, in this case $\triangle\mathbf{r}$ is called an *infinitesimal bearing motion*. An infinitesimal bearing motion corresponding to a translation or a scaling of the whole framework is called *trivial*. The framework $\Theta(\mathcal{G}, \mathbf{f})$ is called *infinitesimally bearing rigid* if all infinitesimal bearing motions are trivial. Intuitively, this means that such frameworks will appear to maintain their shape, regardless of scaling or position, under the dynamics (10b). We now state a rank condition on the bearing rigidity matrix for checking if a given framework exhibits infinitesimal bearing rigidity. Throughout this paper, we will say that a formation is *bearing rigid* implying that it exhibits infinitesimal bearing rigidity.

Theorem 11. *[30] A framework* $\Theta(\mathcal{G}, \mathbf{f})$ *is infinitesimally bearing rigid, if and only if*

$$\mathbf{rank}\left[\mathcal{R}(\Theta)\right] = 2n-3,$$

with the nullspace of $\mathcal{R}(\Theta)$ *spanned by orthogonal vectors* $\mathbf{v}_1 = F^T\begin{bmatrix}\mathbf{1}^T & \mathbf{0}^T\end{bmatrix}^T$, $\mathbf{v}_2 = F^T\begin{bmatrix}\mathbf{0}^T & \mathbf{1}^T\end{bmatrix}^T$, *and* $\mathbf{v}_3 = \tilde{\mathbf{f}}$. *Here,* $F = \begin{bmatrix} I_n \otimes \begin{bmatrix}1 & 0\end{bmatrix} \\ I_n \otimes \begin{bmatrix}0 & 1\end{bmatrix}\end{bmatrix}$ *and* $\tilde{\mathbf{f}}$ *is the underlying unit formation.*

This article has been accepted for publication in a future issue of this journal, but has not been fully edited. Content may change prior to final publication. Citation information: DOI 10.1109/TNSE.2017.2754944, IEEE Transactions on Network Science and Engineering

The vectors $\mathbf{v}_1$, $\mathbf{v}_2$ and $\mathbf{v}_3$ in Thm 11 capture the modes representing the invariance of the bearing measurement to translation in x, translation in y, and scale, respectively.

A consequence of Thm 11 is that the bearing dynamics will converge to a formation parallel to $\mathbf{f}$ if the underlying framework is bearing rigid. Further, as the dynamics are invariant to scale and centroid by Prop. 7 then the dynamics will converge to one of the two formations in $\xi_{\pm}(\mathbf{f}, \boldsymbol{r})$. As discussed in our previous work [1], and summarized in the following corollary of Thm 11, this will almost always be the positively scaled formation $\xi_{+}(\mathbf{f}, \boldsymbol{r})$, with $\xi_{-}(\mathbf{f}, \boldsymbol{r})$ corresponding to an unstable equilibrium point.

Corollary 12. *Let the framework $\Theta(\mathcal{G}, \mathbf{f})$ be infinitesimally bearing rigid. Under the unforced dynamics (10), $\mathbf{r}(t)$ will almost globally exponentially converge to $\xi_{+}(\mathbf{f}, \mathbf{r}_0)$, with the worst-case convergence rate proportional to $\lambda_4\left[\widetilde{\mathcal{R}}(\Theta)^T \widetilde{\mathcal{R}}(\Theta)\right]$.*

4 Formation Acquisition

In this section, we discuss a method to form a desired formation *shape* on n agents over which to apply the weighted bearing-compass dynamics (10). A human operator may provide such a shape, for example from an image as in Fig. 3a, for the purposes of a distributed sensing or coverage problem [31]. Recreating the image using the available n agents, the image can be partitioned into n equal area cells using a Voronoi partitioning algorithm [32], [33]. In doing so, a set of desired agent positions $\mathbf{f} = \begin{bmatrix} \mathbf{f}_1^T & \mathbf{f}_2^T & \cdots & \mathbf{f}_n^T \end{bmatrix}^T$, centered on each cell, is constructed. From Cor. 12, if agent positions $\mathbf{f}$ are coupled with an infinitesimally bearing rigid framework $\Theta(\mathcal{G}, \mathbf{f})$, then agents running the weighted bearing-compass dynamics will converge to $\mathbf{f}$. To this end, this section will focus on selecting links E from a set of available edges, such as those in Fig. 3b, to acquire a favorable graph $\mathcal{G}$, visualized in Fig. 3c from a set of available edges.

It is assumed that the links are selected such that when agents are at $\mathbf{f}$ the graph $\mathcal{G}$ will have short edges to reduce communication costs. This is accomplished by selecting links from a distance graph [9]. This graph, denoted $\mathcal{G}_D = (V, E_D)$, is composed of edges

$$E_D = \{\{i, j\} : \|\mathbf{f}_j - \mathbf{f}_i\| \leq d_{\max}\},$$

where $d_{\max}$ is chosen to be sympathetic to communication range limits of the agents (i.e., wireless signal strength or a distance such that a monocular camera can still resolve neighboring agents).

We will use the desired agent positions $\mathbf{f}$ and the feasible edge set E_D to select some $E \subseteq E_D$ such that the dynamics (10) will both converge and be optimal over various metrics, such as maximizing convergence.

In §4.1, we will explore a necessary and sufficient condition on the bearing rigidity matrix $\mathcal{R}(\Theta)$ for the dynamics to converge. More specifically, we will select an edge set $E \subseteq E_D$ such that the conditions on infinitesimal bearing rigidity, outlined in Thm 11, are met, which means the formation satisfies $\mathbf{rank}\left[\mathcal{R}(\Theta)\right] = 2n - 3$. It is assumed that $d_{\max}$ is sufficiently large so that such a selection E with this criteria exists.

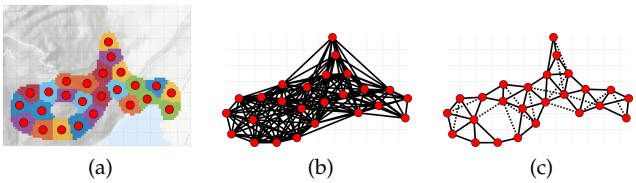

Figure 3: a) A human operator draws the formation shape on a map, and a Voronoi partitioning of the agents is computed. b) A distance graph is constructed which provides the edges we will select from. c) Edges are selected to ensure the formation is bearing rigid, and is as performant as possible given different performance metrics. Dotted edges represent additional edges past what is needed for infinitesimal bearing rigidity, as extra edges typically improve performance.

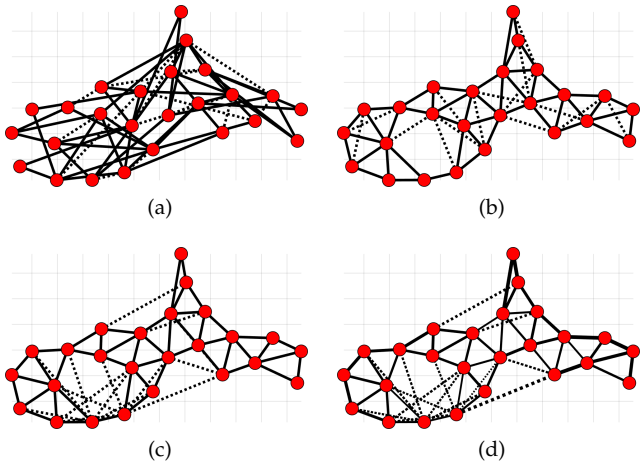

Figure 4: Greedy edge selection under metrics: a) $f_r(S)$, b) $f_r(S) + \alpha f_t(S)$ and c) $f_r(S) + \alpha f_t(S)$ until the graph is infinitesimally rigid and then $f_\ell(S)$. (d) Edge weight selection using Alg. 2 with the edge set from Fig. 4c. Solid lines indicate edge required for infinitesimal rigidity using Alg. 1 and dashed indicate additional edges to improve convergence using greedy selection. Edge thickness indicates the relative edge weights.

While our formation edge set must be bearing rigid, we would also like the set to promote good performance of the dynamics. We can add additional terms to the edge selection to promote this, which we will explore in §4.2. Further, we might be given a set of edges that we must use, in which case we can optimize the weights of those edges to further improve performance. This is explored in §4.3.

An example of such a refinement can be seen in Fig. 4, where the edges have been selected from those in the distance graph in Fig. 3b.

Submodularity is key to our approach to the edge selection problem. In particular, the theorem below serves as the workhorse for the results that follow.

Theorem 13. *Let $S \subseteq E$ and*

$$Q(S) = U(S)^T U(S),$$

This article has been accepted for publication in a future issue of this journal, but has not been fully edited. Content may change prior to final publication. Citation information: DOI 10.1109/TNSE.2017.2754944, IEEE Transactions on Network Science and Engineering

where $U(S) = (I(S \cup S_0) \otimes I_d)\, U(E)$, $I(T)$ represents the T columns of the identity matrix and S_0 is the columns of $U(E)$ associated with $S = \{\emptyset\}$. Then the following are submodular functions:

a) $f_r(S) = \mathbf{rank}\,[Q(S)]$

b) $f_t(S) = \mathbf{trace}\,[Q(S)]$

c) $f_\ell(S) = \mathbf{logdet}\,[Q(S)]$ *for* $Q(S) \succ 0$.

Furthermore, $f_t(S)$ is, in fact, modular.

Proof: (a) We observe that

$$\mathbf{rank}\,[Q(S)] = \mathbf{rank}\left[U(S)^T U(S)\right] = \mathbf{rank}\left[U(S)^T\right].$$

The matrix $U(S)$ corresponds to the $S \cup S_0$ column pairs of $U(E)$. Maximizing $f_r(S)$ over S is then equivalent to selecting the 2-pair columns of each $s \in S$ in $U(E)$ that maximizes the rank. This is the standard matroid rank problem and f_r is submodular [24].

In support of (b) and (c), observe that

$$\begin{aligned} Q(S) &= U(S)^T U(S) \\ &= U(E)^T \left(I(S \cup S_0) \otimes I_2\right)^T \left(I(S \cup S_0) \otimes I_2\right) U(E) \\ &= U(E)^T \sum_{s=\{\emptyset\}, s \in S} \left[\left(I(\{s\}) \otimes I_2\right)^T \left(I(\{s\}) \otimes I_2\right)^T\right] U(E) \\ &= Q(\emptyset) + \sum_{s \in S} Q(\{s\}). \end{aligned} \tag{16}$$

(b) As $\mathbf{trace}\,[Q(S)] = \sum_{s \in S} \mathbf{trace}\,[Q(\{s\})]$ it follows that $\mathbf{trace}\,[Q(S)]$ is modular.

(c) For $M \succ 0$ and $N, P \succeq 0$ then $\mathbf{det}(M)\,\mathbf{det}(M+N+P) \leq \mathbf{det}(M+N)\mathbf{det}(M+P)$ [34]. As $\mathbf{log}(\cdot)$ is an increasing function then

$$\begin{aligned} 0 \leq\ & \mathbf{log}(\mathbf{det}(M+N)\mathbf{det}(M+P)) \\ & - \mathbf{log}(\mathbf{det}M\mathbf{det}(M+N+P)) \\ & \leq \mathbf{logdet}(M+N) + \mathbf{logdet}(M+P) \\ & - (\mathbf{logdet}M + \mathbf{logdet}(M+N+P)) \\ & \leq \mathbf{logdet}(M+P)) - \mathbf{logdet}M) \\ & - (\mathbf{logdet}(M+N+P) - \mathbf{logdet}(M+N)). \end{aligned} \tag{17}$$

Consider now $A \subseteq B \subseteq \mathcal{S}$ and $s \notin B$. Assume that $Q(A) \succ 0$ as $Q(S)$ is formed by the sum of positive semidefinite matrices, then $Q(B) - Q(A), Q(\{s\}) \succeq 0$. Let $M = Q(A)$, $N = Q(B) - Q(A)$, $P = Q(\{s\})$ and applying (16) and (17) as

$$\begin{aligned} 0 \leq\ & \mathbf{logdet}(Q(A) + Q(\{s\}) - \mathbf{logdet}Q(A) \\ & - (\mathbf{logdet}(Q(B) + Q(\{s\}) - \mathbf{logdet}Q(B)) \\ & \leq \mathbf{logdet}Q(A \cup \{s\}) - \mathbf{logdet}Q(A) \\ & - (\mathbf{logdet}Q(B \cup \{s\}) - \mathbf{logdet}Q(B)). \end{aligned}$$

Hence, by Def. 3, $\mathbf{logdet}\,[Q(S)]$ is submodular. □

4.1 Edge Selection for Bearing Rigidity

From Cor. 12, a necessary condition for dynamics (10) to converge to a formation similar to $\mathbf{f}$ is that the framework Θ is infinitesimally bearing rigid. From Thm 11, it is then desirable to select a subset of edges $S \subseteq E_D$ so that

Algorithm 1 Select edges which guarantee infinitesimal bearing rigidity.

Input: Graph to refine: $\mathcal{G}_D = (V, E_D)$
Ensure: $\mathbf{rank}[\mathcal{R}(E_D)] = 2n - 3$
Input: Submodular set function: $f(S), S \subseteq E_D$
1: $S \leftarrow \emptyset$
2: **while** $\mathbf{rank}[\mathcal{R}(S)] < 2n - 3$ **do**
3: $\quad e^* = \underset{e \in E_D \setminus S}{\mathbf{argmax}} \left[f(S \cup \{e\}) - f(S)\right]$ ‡
4: $\quad S \leftarrow (S \cup \{e^*\})$
5: **end while**
6: **return** S

$\mathbf{rank}\,[\mathcal{R}] = 2n - 3$. Representing the rigidity matrix as a matrix valued function with respect to the edges S then

$$\mathcal{R}(S) = \frac{\partial \hat{\mathbf{g}}(S)}{\partial \mathbf{f}}$$

where $\hat{\mathbf{g}}(S) = \begin{bmatrix} \hat{\mathbf{f}}_{s_1}^T & \hat{\mathbf{f}}_{s_2}^T & \cdots \end{bmatrix}^T$, for $S = \{s_1, s_2, \dots\} \subseteq E_D$. The unitless rigidity matrix $\widetilde{\mathcal{R}}(S)$ is similarly defined. We leverage this rank property in the following proposition.

Proposition 14. *The set function*

$$f_r(S) = \mathbf{rank}\,[\mathcal{R}(S)] \tag{18}$$

for $S \subseteq E_D$ is submodular.

Proof: This result follows directly from Thm 13.a by letting $S_0 = \{\emptyset\}$ and

$$\begin{aligned} U(S) &= \mathcal{R}(S) \\ &= (I(S \cup S_0) \otimes I_2)\mathcal{R}(E_D). \end{aligned}$$

□

Since we have shown that the rank of the bearing rigidity matrix $\mathcal{R}$ is submodular over the underlying edge set E, we can apply Thm 5 to select edges in a greedy fashion, leading to an infinitesimally bearing rigid formation. This process is described in Alg. 1 and demonstrated in Fig. 4a with the selection of the solid edges to acquire a bearing rigid formation. In fact, as the rank increases by at most one with the addition of an edge, the greedy method corresponds to the check and selection of linear independent columns of $\mathcal{R}(E_D)$. Hence, Alg. 1 will attain an infinitesimally bearing rigid formation with the minimal number of edges, namely $2n - 3$.

4.2 Edge Selection for Convergence

In §4.1, we showed how to select edges such that the resulting formation is bearing rigid. However, in large formations with many possible edges, it is likely that many such selections will meet this minimum rank requirement, and some selections might offer better performance than others. In this section, we explore ways to promote formation convergence as a part of the edge selection process. The underlying Lyapunov function and the associated Lyapunov rate from Thm 10 is $V = \frac{1}{2}\mathbf{z}^T\mathbf{z}$ and $\dot{V} \leq -S(\mathbf{f})^{-1}\mathbf{z}^T Q\mathbf{z}$, respectively.

‡. If, as in Thm 5, $R > 1$, then this line will select the subset $e \subseteq E_D \setminus S$ such that $|e| = R$ if $|E_D \setminus S| \geq R$ and $|e| = |E_D \setminus S|$ otherwise.

This article has been accepted for publication in a future issue of this journal, but has not been fully edited. Content may change prior to final publication. Citation information: DOI 10.1109/TNSE.2017.2754944, IEEE Transactions on Network Science and Engineering

Explicitly encoding the edges $S \subseteq E_D$ that contribute to Q then

$$Q(S) = \widetilde{\mathcal{R}}(S)^T \mathcal{D}_{\bar{k}(S)} \left[m_{\bar{k}}^2 I_2\right] \widetilde{\mathcal{R}}(S), \tag{19}$$

where $\widetilde{\mathcal{R}}(S) := (I(S) \otimes I_2)\, \widetilde{\mathcal{R}}$, $m_{\bar{k}}^2$ is defined as in Thm 10, $\mathcal{D}_{\bar{k}(S)} \left[m_{\bar{k}}^2 I_2\right] := (I(S) \otimes I_2)\, \mathcal{D}_{\bar{k}} \left[m_{\bar{k}}^2 I_2\right] (I(S) \otimes I_2)^T$, and $\widetilde{\mathcal{R}}$ and $\mathcal{D}_{\bar{k}} \left[m_{\bar{k}}^2 I_2\right]$ are constructed from the edge set E_D.

The worst-case convergence rate to the null-space of Q is dictated by the smallest nonzero eigenvalue of Q. This also dictates the exponential convergence envelope of the dynamics. The other non-zero eigenvalues of Q also play a role in describing the convergence of the dynamics. Edge selection based on measures of these eigenvalues has the effect of improving the overall dynamics performance and is the edge optimization criteria for this section.

The first considered measure is **trace** $[Q]$, which is proportional to the instantaneous average convergence envelope of the dynamics at time t when the initial error is $\|\mathbf{z}(t)\|$ is sampled evenly on the unit circle. This follows from the fact that for a fixed scale $S(\mathbf{f})^{-1}$,

$$\begin{aligned}
&\frac{d}{dt}\mathbb{E}_{\|\mathbf{z}(t)\|=1} V(z(t)) \\
&\leq -S(\mathbf{f})^{-1}\, \mathbb{E}_{\|\mathbf{z}(t)\|=1} \mathbf{z}^T(t)\, Q \mathbf{z}(t) \\
&= -S(\mathbf{f})^{-1}\, \frac{1}{2n} \sum_{i=1}^{n} \lambda_i(Q) \mathbb{E}_{\|\mathbf{z}(t)\|=1} \mathbf{z}^T(t)\, \mathbf{z}(t) \\
&= \left(\frac{-1}{nS(\mathbf{f})} \textbf{trace}\,[Q]\right) \mathbb{E}_{\|\mathbf{z}(t)\|=1} V(\mathbf{z}(t)).
\end{aligned}$$

Consequently, a larger **trace** $[Q]$ will speed up the average convergence rate envelope.

An attraction of this measure is that it is modular with respect to the edge selection problem on the graph. This feature is formalized in the following proposition.

Proposition 15. *Let $Q(S)$ be defined as in (19); then the set function*

$$f_t(S) = \textbf{trace}\,[Q(S)] \tag{20}$$

for $S \subseteq E_D$ is modular.

Proof: The proof follows from Thm 13.b by letting $S_0 = \{\emptyset\}$ and

$$\begin{aligned}
U(S) &= \mathcal{D}_{\bar{k}(S)} \left[m_{\bar{k}} I_2\right] \widetilde{\mathcal{R}}(S) \\
&= (I(S) \otimes I_2)\, \mathcal{D}_{\bar{k}} \left[m_{\bar{k}}^2 I_2\right] (I(S) \otimes I_2)^T (I(S) \otimes I_2)\, \widetilde{\mathcal{R}} \\
&= (I(S) \otimes I_2)\, \mathcal{D}_{\bar{k}} \left[m_{\bar{k}}^2 I_2\right] \widetilde{\mathcal{R}} \\
&= (I(S) \otimes I_2)\, \mathcal{D}_{\bar{k}(E_D)} \left[m_{\bar{k}} I_2\right] \widetilde{\mathcal{R}}(E_D).
\end{aligned}$$

□

A boon of the modularity of **trace** $[Q]$ is that the greedy selection of edges under this measure provides the optimal edge selection. Interestingly, **trace** $[Q]$ is independent of the unitless rigidity matrix $\widetilde{\mathcal{R}}(S)$. This becomes apparent by manipulating the trace of a single edge $\{s\} \in E_D$, indicating the sth row of H by $H_{\bar{s}}$; then

$$\begin{aligned}
f_t(\{s\}) &= \textbf{trace}[\widetilde{\mathcal{R}}(\{s\})^T \mathcal{D}_{\bar{k}(\{s\})} \left[m_{\bar{k}}^2 I_2\right] \widetilde{\mathcal{R}}(\{s\})] \\
&= \textbf{trace}[(H_{\bar{s}} \otimes I_2) \mathcal{D}_{\bar{k}(\{s\})} \left[m_{\bar{k}}^2 I_2\right] (H_{\bar{s}}^T \otimes I_2)] \\
&= \textbf{trace}[m_{\bar{s}}^2 (\begin{bmatrix} 1 \\ -1 \end{bmatrix} \otimes I_2) P_{\bar{s}}^2 (\begin{bmatrix} 1 & -1 \end{bmatrix} \otimes I_2)] \\
&= \textbf{trace}[m_{\bar{s}}^2 (\begin{bmatrix} 1 & -1 \end{bmatrix} \begin{bmatrix} 1 \\ -1 \end{bmatrix} \otimes I_2) P_{\bar{s}}] \\
&= \textbf{trace}[2 m_{\bar{s}}^2 P_{\bar{s}}] = 2 m_{\bar{s}}^2,
\end{aligned} \tag{21}$$

and using the property that $f_t(S) = \sum_{s \in S} f_t(\{s\}) = 2 \sum_{s \in S} m_{\bar{s}}^2$, as $f_t(S)$ is a modular function. The measure is therefore solely dependent on the lengths $\left\|\tilde{\mathbf{f}}_{\bar{k}}\right\|$ and weights $w_{\bar{k}}$ of the selected edges, and the initial condition $\mathbf{r}_0$. Figure 5a plots the function $m_{\bar{k}}^2$ for an unweighted edge. For the regime $\left\|\tilde{\mathbf{f}}_{\bar{k}}\right\| \geq \|\mathbf{z}_0\|\, S(\mathbf{f})^{-1}$ for all edges $\bar{k}$, or equivalently $\|\mathbf{f}_{\bar{k}}\| \geq \|\mathbf{r}_0 - \xi_+(\mathbf{f}, \mathbf{r}_0)\|$, then smaller $\left\|\tilde{\mathbf{f}}_{\bar{k}}\right\|$ corresponds to a large $m_{\bar{k}}^2$ and therefore a larger **trace** $[Q]$, i.e., smaller edges in the final formation shape are preferable. For the regime $\left\|\tilde{\mathbf{f}}_{\bar{k}}\right\| \leq \|\mathbf{z}_0\|\, S(\mathbf{f})^{-1}$, the reverse is true. Examining convergence rate close to the equilibrium, namely when

$$\|\mathbf{r}_0 - \mathbf{f}\| \leq \min_{\bar{k}} \|\mathbf{f}_{\bar{k}}\|, \tag{22}$$

then the optimal q-edge selection to maximize **trace** $[Q]$ would be to select the q shortest edges $\left\|\tilde{\mathbf{f}}_{\bar{k}}\right\|$.

As $f_t(S)$ is independent of $\widetilde{\mathcal{R}}(S)$, it will not necessarily favor a maximum rank rigidity matrix which is necessary to acquire the desired formation shape. An alternative is to use this result in conjunction with the submodular rank measure described in Prop. 14. This can be achieved by applying the additive submodular property of Prop. 4 to form the new submodular function

$$f(S) = f_r(S) + \alpha f_t(S), \tag{23}$$

where $\alpha > 0$.

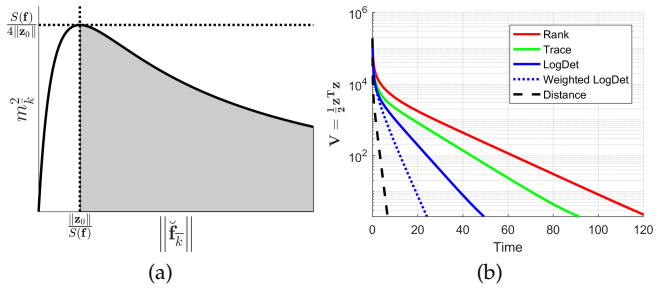

(a) (b)

Figure 5: a) Curve for $m_{\bar{k}}^2$ versus $\left\|\tilde{\mathbf{f}}_{\bar{k}}\right\|$ for an unweighted edge, i.e., $w_{\bar{k}} = 1$, given desired formation $\mathbf{f}$ with initial error $\mathbf{z}_0$. b) Average potential over 100 random initial conditions, where the rank curve is the formation from Fig. 4a, trace curve is the formation from Fig. 4b, log det curve is the formation from Fig. 4c, the weighted log det curve is the formation from Fig. 4d and the inclusion of all edges E_D in the formation from Fig. 3b.

This article has been accepted for publication in a future issue of this journal, but has not been fully edited. Content may change prior to final publication. Citation information: DOI 10.1109/TNSE.2017.2754944, IEEE Transactions on Network Science and Engineering

So as to encourage the minimal number of required edges for convergence to the desired formation associated with $f_r(S) = 2n-3$, then it may be desired to preferentially select the rigidity rank measure over the trace measure. To this end, α can be selected to ensure that $f_r(S)$, an integer, dominates $f(S)$. Specifically, when $\alpha < 1/f_t(E_D)$ then as $f_t(S)$ is monotonically increasing $\alpha f_t(S) \in [0,1)$ for all $S \subseteq E_D$. Hence, an edge $e \in E_D \setminus S$ will be selected if it increases rank in preference to if it increases trace as [2]

$$f_r(S \cup \{e\}) - f_r(S) \geq 1 \geq \alpha \left(f_t(S \cup \{e\}) - f_t(S)\right).$$

The effect of this choice results in the trace measure "breaking ties" if there is more than one choice of edge which increases rank when using the greedy selection heuristic for rank in Alg. 1. After sufficient edges S_R have been added to the graph such that the rigidity matrix is maximum rank, i.e., $\mathbf{rank}\left[\mathcal{R}(S_R)\right] = \mathbf{rank}\left[Q(S_R)\right] = 2n-3$, then to further improve performance it may be desired to add additional edges $S \in E_D \setminus S_R$. The $\mathbf{trace}\left[Q(S_R \cup S)\right]$ is one measure to accomplish this result.

The solid edges in Fig. 4b indicate an infinitesimally rigid graph formed under greedy selection for $f_r(S) + \alpha f_t(S)$ with α sufficiently small such that $\alpha < 1/f_t(E_D)$. Comparing the solid edges in Fig. 4a, i.e., selection only under rank, to Fig. 4b a formation with shorter edges is acquired. Additional edges to improve performance under $f_r(S)$ and $f_r(S) + \alpha f_t(S)$ are indicated in Figs. 4a and 4b, respectively. Figure 5b shows the improved convergence rate of the edge selection under both the trace and rank measure compared to the rank measure alone.

A limitation of the measure in Eq. (23) is that, as it is based on the average convergence, it does not favor improving the worst case convergence. The worst case convergence is dictated by the smallest non-zero eigenvalue of Q, namely $\lambda_4(Q)$. The set function $f(S) = \lambda_4(Q(S_R \cup S))$ is not a submodular function, however, so does not provide greedy guarantees when Alg. 1 is applied. An alternative measure, which promotes increasing the smallest eigenvalues of a matrix, is $\sum_{i=4}^{2n} \mathbf{log}\lambda_i(Q(S_R \cup S))$. From the discussion on the nullspace of $\mathcal{R}$ in Thm 11, note that $\hat{\mathbf{v}}_1, \hat{\mathbf{v}}_2$ and $\hat{\mathbf{v}}_3$ span the nullspace of $Q(S_R)$ with unitary eigenvalues, i.e., $Q(S_R) + \sum_{j=1}^{3} \hat{\mathbf{v}}_j \hat{\mathbf{v}}_j^T$ is full rank and $\mathbf{log}\lambda_n(\hat{\mathbf{v}}_j \hat{\mathbf{v}}_j^T) = \mathbf{log}(1) = 0$. Hence, for $\mathbf{rank}\left[Q(S_R)\right] = 2n-3$ it follows that

$$\begin{aligned}
&\sum_{i=4}^{2n} \mathbf{log}\lambda_i(Q(S_R \cup S)) \\
&= \sum_{i=4}^{2n} \mathbf{log}\lambda_i(Q(S_R \cup S)) + \sum_{j=1}^{3} \mathbf{log}\lambda_n(\hat{\mathbf{v}}_j \hat{\mathbf{v}}_j^T) \\
&= \sum_{i=1}^{2n} \mathbf{log}\lambda_i[Q(S_R \cup S) + \sum_{j=1}^{3} \hat{\mathbf{v}}_j \hat{\mathbf{v}}_j^T] \\
&= \mathbf{tracelog}[Q(S_R \cup S) + \sum_{j=1}^{3} \hat{\mathbf{v}}_j \hat{\mathbf{v}}_j^T]^{\dagger\dagger} \\
&= \mathbf{logdet}[Q(S_R \cup S) + \sum_{j=1}^{3} \hat{\mathbf{v}}_j \hat{\mathbf{v}}_j^T].
\end{aligned}$$

2. The same result follows if batches of edges are added, i.e., $R > 1$in Thm 5.

The following proposition describes the submodularity of $\sum_{i=4}^{2n} \mathbf{log}\lambda_i(Q)$ providing the necessary features to guarantee the suboptimal greedy selection performance of Thm 5.

Proposition 16. *Let $Q(S)$ be defined as in (19); the set function*

$$f_\ell(S) = \mathbf{logdet}[Q(S_R \cup S) + \sum_{i=1}^{3} \hat{\mathbf{v}}_i \hat{\mathbf{v}}_i^T], \tag{24}$$

for $S \subseteq E_D \setminus S_R$ and where $\mathbf{rank}\left[f_\ell(\emptyset)\right] = \mathbf{rank}\left[Q(S_R)\right] = 2n-3$, is submodular.

Proof: Following similarly to the proof of Prop. 15, then

$$\begin{aligned}
U(S) &= \begin{bmatrix} \mathcal{D}_{\bar{k}(S_R \cup S)}\left[m_{\bar{k}} I_2\right] \widetilde{\mathcal{R}}(S_R \cup S) \\ \sum_{i=1}^{3} \hat{\mathbf{v}}_i \hat{\mathbf{v}}_i^T \end{bmatrix} \\
&= I(S \cup S_R \cup T) \otimes I_2 \begin{bmatrix} \mathcal{D}_{\bar{k}(S_R \cup E_D)}\left[m_{\bar{k}} I_2\right] \widetilde{\mathcal{R}}(S_R \cup E_D) \\ \sum_{i=1}^{3} \hat{\mathbf{v}}_i \hat{\mathbf{v}}_i^T \end{bmatrix} \\
&= (I(S \cup S_0) \otimes I_2) U(E_D),
\end{aligned}$$

where $T = \{|E_D|+1, |E_D|+2, |E_D|+3\}$ and $S_0 = S_R \cup T$. Further as $\sum_{i=1}^{3} \hat{\mathbf{v}}_i \hat{\mathbf{v}}_i^T$ is an idempotent matrix then $U^T(S)U(S) = Q(S_R \cup S) + \sum_{i=1}^{3} \hat{\mathbf{v}}_i \hat{\mathbf{v}}_i^T$. Therefore, $U(S)$ is in the necessary form to apply Thm 13.c and so the result follows. □

Consider the infinitesimally rigid formation acquired under the selection measure $f_r(S) + \alpha f_t(S)$ indicated with solid edges in Fig. 4a. As $\mathbf{rank}\left[Q(S_R)\right] = 2n-3$ then additional edges can be selected under the measure $f_\ell(S)$ to improve performance. Fig. 4c indicates the greedy selection of an additional 15 edges with dashed edges. The relative performance between the three measures is shown in Fig. 5b with $f_\ell(S)$ outperforming the other two.

4.3 Edge Weight Selection

Once an edge set E has been selected to achieve infinitesimal bearing rigidity, additional performance improvement can also be garnered if edge weights $\mathbf{w}$ can be designed non-uniformly. Assuming the weights are positive continuous variables for certain selection criteria these can be optimized using convex optimization. Examining dynamics (10b), as $\left\|(\hat{\mathbf{r}}_{ij}^T \hat{\mathbf{f}}_{ij}^{\perp}) \hat{\mathbf{r}}_{ij}^{\perp}\right\| \leq 1$, then $\left\|\mathbf{u}_{(ij)}\right\| \leq w_{ij}$ and so the edge weight w_{ij} is akin to the maximum available control effort available to correct for errors induced by the edge $\{i,j\}$. Not surprisingly, increasing edge weights has the effect of increasing the convergence rate of the dynamics. This is captured more explicitly through Cor. 12 where the worst case convergence is dictated by the smallest non-zero eigenvalue of $Q(\mathbf{w})$, namely $\lambda_4(Q(\mathbf{w}))$, and the edge weights appear linearly in the term $m_{\bar{k}}^2(w_{\bar{k}})$ within the definition of Q. Balancing the maximum control effort available at each node, defined as $u_{\max}$, and maximizing $\lambda_4(Q(w))$ then an equivalent optimization problem is:

$$\begin{aligned}
&\underset{\mathbf{w}}{\text{maximize}}\ \lambda_4(Q(\mathbf{w})) \\
&\qquad \text{s.t. } w_{\bar{k}} \geq 0,\ \sum_{j \in N(i)} w_{ij} \leq u_{\max}.
\end{aligned} \tag{25}$$

††. For matrix M, $\mathbf{log}[M]$ denotes to the matrix logarithm of M.

This article has been accepted for publication in a future issue of this journal, but has not been fully edited. Content may change prior to final publication. Citation information: DOI 10.1109/TNSE.2017.2754944, IEEE Transactions on Network Science and Engineering

The control effort cap in (25) can be represented in terms of the incidence matrix of the graph as $\left|H^T\right|\mathbf{w} \leq u_{\max}\mathbf{1}$, where $|\cdot|$ for a matrix indicates the element-wise absolute value.

Applying a similar approach to Prop. 16 to remove the nullspace of Q then

$$\lambda_4(Q) = \lambda_1(Q + \beta\sum_{i=1}^{3}\hat{\mathbf{v}}_i\hat{\mathbf{v}}_i^T). \tag{26}$$

It is assumed that β is large enough to shift the eigenvalues associated with $\sum_{i=1}^{3}\hat{\mathbf{v}}_i\hat{\mathbf{v}}_i^T$ above $\lambda_4(Q)$, i.e., $\beta \geq \lambda_4(Q)$. A sufficiently large β can be found by examining an upper bound of $\frac{1}{2n-3}\mathbf{trace}\,[Q]$ which is the average over the nonzero eigenvalues of Q with

$$\begin{aligned}\lambda_4(Q) &\leq \frac{1}{2n-3}\sum_{i=4}^{2n}\lambda_i(Q) = \frac{1}{2n-3}\mathbf{trace}\,[Q]\\ &= \frac{1}{2n-3}2\sum_{\bar{k}=1}^{m}m_{\bar{k}}^2 \text{ (from equality (21))}\\ &\leq \frac{2}{2n-3}\sum_{\bar{k}=1}^{m}w_{\bar{k}}\frac{S(\mathbf{f})}{4\left\|z_0\right\|} \text{ (from upper bound in Fig. 5a)}\\ &\leq \frac{S(\mathbf{f})}{2\left\|z_0\right\|}\frac{1}{2n-3}\frac{n}{2}u_{\max} = \frac{nu_{\max}}{4\left(2n-3\right)}\frac{S(\mathbf{f})}{\left\|z_0\right\|} := \beta,\end{aligned}$$

where the final inequality follows from the maximum control cap as

$$\sum_{\bar{k}=1}^{m}w_{\bar{k}} = \frac{1}{2}\sum_{i=1}^{n}\sum_{j\in N(i)}w_{ij} \leq \frac{1}{2}\sum_{i=1}^{n}u_{\max} \leq \frac{n}{2}u_{\max}.$$

From the additive property (16) over the edges of Q then

$$\begin{aligned}Q &= \sum_{s\in E}Q(\{s\})\\ &= \sum_{s\in E}\widetilde{\mathcal{R}}\left(\{s\}\right)^T\mathcal{D}_{\bar{k}(\{s\})}\left[m_{\bar{k}}^2 I_2\right]\widetilde{\mathcal{R}}\left(\{s\}\right)\\ &= \sum_{s\in E}w_{\bar{s}}\widetilde{\mathcal{R}}\left(\{s\}\right)^T\left[\frac{\left\|\tilde{\mathbf{f}}_{\bar{s}}\right\|}{\left(S\left(\mathbf{f}\right)^{-1}\left\|\mathbf{z}_0\right\| + \left\|\tilde{\mathbf{f}}_{\bar{s}}\right\|\right)^2}I_2\right]\widetilde{\mathcal{R}}\left(\{s\}\right)\\ &= \sum_{s\in E}w_{\bar{s}}Q_u(\{s\}),\end{aligned}$$

where $Q_u\left(\{s\}\right)$ is the matrix representing the unweighted contribution of edge $s \in E$. Hence, the maximization of $\lambda_4(Q)$ using (26) can be represented as a linear matrix inequality and solved as a convex optimization presented in Alg. 2.

We note that one reasonable strategy using what we have developed is to do an initial edge selection based on the methods in §4.1 and §4.2, then apply Alg. 2 to refine the chosen edge weights. An example of the edge weight selection is shown in Fig. 4d applied to the edges of Fig. 4c. The improved convergence rate can be seen in Fig. 5b.

5 Formation Manipulation

In our previous work [6] we studied the performance of the *forced* dynamics (10a). External signals were applied from

Algorithm 2 Algorithm to maximize $\lambda_4\left(Q\right)$ with respect to the weight vector $\mathbf{w}$ given a fixed edge set E.

$$\begin{aligned}&\underset{\mathbf{w}}{\text{maximize}}\ \delta\\ &\text{s.t.}\ \sum_{s\in E}w_{\bar{s}}Q_u(\{s\}) + \beta\sum_{i=1}^{3}\hat{\mathbf{v}}_i\hat{\mathbf{v}}_i^T \succeq \delta I,\\ &\quad\mathbf{w} \geq \mathbf{0},\ \left|H^T\right|\mathbf{w} \leq u_{\max}\mathbf{1}\end{aligned}$$

leader agents $V_\ell \subseteq V$ with $\tilde{\mathbf{u}}_i \neq 0$, where the selection criteria of a "favorable" leader was based on the leader's ability to translate or scale a bearing-constrained formation. The considered form of $\tilde{\mathbf{u}}_i$ was an impulse signal. In this section, we adapt the tools developed in the previous sections to select leaders which have external signals that "ground" the formation to a certain centroid and scale given information from a set of anchors which behave as stationary neighbors. These *leader agents* will manipulate the formation as a whole, so we can acquire the desired formation scale and centroid. Taking a similar approach to Shames and Summers [28], we assume there are some external *anchors* that act as additional bearing constraints to any agent that can sense them. There are many examples of such signals like the VHF omni-directional range (VOR) radio navigation system used by aircraft, localizing from signals of opportunity like CDMA cellular towers [35], or simply letting a subset of agents have access to their position using GPS so they can measure their bearing offset from locations set *a priori*. This anchored setup complements the work by Zhao and Zelazo [13], [20] which considers a set of anchor nodes that are native to the graph.

Let V_a be the set of n_a *anchor nodes* with corresponding positions $\mathbf{f}_a \in \mathbb{R}^{2n_a}$. Let $E_a\left(S\right) = \{\{i,j\} : i \in S, j \in V_a\}$ be the set of edges between anchors and the leaders in set $S \subseteq V$. This set represents the possible bearing measurements a leader agent can make. In this section, we will still be selecting a subset of edges, but in contrast to previous sections, we will do so by selecting edges connected to a subset of the agents. This will result in selecting a subset of the anchor edges via selecting leaders resulting in a system which is "full rank" with respect to an augmented rigidity matrix and exhibits "good performance".

Specifically, leaders have access to a family of n_a *anchor* reference positions. The ith anchor's position is denoted as $\mathbf{a}_i \in \mathbb{R}^2$. The graph $\mathcal{G}$ is extended to include anchor nodes V_a, or cardinality n_a, and m_a anchored edges $\{i,j\}$ with weights w_{ij} for all $i \in V_a$ and $j \in V_\ell$ with the extended neighborhood of agents V_ℓ denoted as $\mathcal{N}_a$. The agent's position vector $\mathbf{r}$ is augments with the anchor positions with $\mathbf{r}_{n+i} = \mathbf{a}_i$ for $i = 1,\ldots,n_a$ and the desired formation $\mathbf{f}$ is similarly augmented with $\mathbf{f}_{n+i} = \mathbf{a}_i$. The leader agents forced signal is then defined using the new bearing measurements to the anchors as

$$\tilde{\mathbf{u}}_i = \sum_{j\in\mathcal{N}_a(i)}w_{ij}(\hat{\mathbf{r}}_{ij}^T\hat{\mathbf{f}}_{ij}^{\perp})\hat{\mathbf{r}}_{ij}^{\perp}. \tag{27}$$

The attraction of this form of external leader signal is that much of the machinery established in the previous section can be adapted to examine the *anchored* properties of these

This article has been accepted for publication in a future issue of this journal, but has not been fully edited. Content may change prior to final publication. Citation information: DOI 10.1109/TNSE.2017.2754944, IEEE Transactions on Network Science and Engineering

dynamics. The first notion is the anchored rigidity matrix $\mathcal{R}_a \in \mathbb{R}^{2(m+m_a)\times 2(n+n_a)}$, can be formed as $\mathcal{R}_a(\Theta) := \frac{\partial \hat{\mathbf{g}}}{\partial \mathbf{f}}$. Noting that $\left[\frac{\partial \hat{\mathbf{g}}}{\partial \mathbf{f}}\right]_{ij} = 0$ for $j \in V_a$, as the anchors nodes are effectively grounded, then

$$\mathcal{R}_a = \begin{bmatrix} \mathcal{R} & \mathbf{0} \\ \frac{\partial \hat{\mathbf{g}}_a}{\partial \mathbf{f}} & \mathbf{0} \end{bmatrix}$$

where $\mathcal{R}$ is the rigidity matrix of the unanchored formation and $\hat{\mathbf{g}}_a = \begin{bmatrix} \hat{\mathbf{f}}_{\overline{m+1}} & \hat{\mathbf{f}}_{\overline{m+2}} & \cdots & \hat{\mathbf{f}}_{\overline{m+m_a}} \end{bmatrix}$. The anchored unitless rigidity matrix $\widetilde{\mathcal{R}}_a$ is defined similarly to the unitless rigidity matrix $\widetilde{\mathcal{R}}$. Consequently, the anchors can serve as a method to remove the nullspace associated with the centroid and scale of $\mathcal{R}$. When sufficient bearing measurements are added to the dynamics, through the addition of anchors and leaders to define a unique formation $\mathbf{f}$, then the framework Θ is called *anchored* infinitesimally bearing rigid. This property manifests itself as a rank property summarized in the following theorem.

Theorem 17. *For a framework to be anchored infinitesimally bearing rigid, we must have that*

$$\mathbf{rank}\left[\mathcal{R}_a(\Theta)\right] = 2n.$$

As the addition of an anchor grounds at most two dimensions in the null space of $\mathcal{R}$, at least two anchors are needed, with associated leader agent edges, for an infinitesimally bearing rigid framework to become an anchored infinitesimally bearing rigid framework. Not surprisingly, for a anchored infinitesimally bearing rigid formation then the dynamics will converge exponentially to the unique formation $\mathbf{f}$. The proof of this property echoes that of Thm 10 using Thm 17. The result is summarized in the following without proof, leveraging the property $\mathbf{rank}\left[\mathcal{R}_a\right] = 2n$ to show that the dynamics converge to a unique $\mathbf{f}$, rather than a formation dependent on the initial conditions as in Cor. 12.

Theorem 18. *Let the framework $\Theta(\mathcal{G}, \mathbf{f})$ be anchored infinitesimally bearing rigid. Under the forced dynamics (10) with (27), a Lyapunov function is $V = \frac{1}{2}\mathbf{z}^T\mathbf{z}$, where $\mathbf{z} = \mathbf{r} - \mathbf{f}$, with associated Lyapunov rate bounded as*

$$\dot{V} \leq S(\mathbf{f})^{-1}\mathbf{z}^T\widetilde{\mathcal{R}}_a^T\mathcal{D}_{\bar{k}}\left[m_{\bar{k}}^2 I_2\right]\widetilde{\mathcal{R}}_a\mathbf{z} := -S(\mathbf{f})^{-1}\mathbf{z}^T Q_a\mathbf{z},$$

where $m_{\bar{k}}^2(\mathbf{r}_0)$ is as defined in Thm 10. Consequently, $\mathbf{r}(t)$ will globally exponentially converge to $\mathbf{f}$.

5.1 Leader Selection for Anchor Rigidity

As for the unforced dynamics, it is important to reason about effective graph topologies that meet the requirements for convergence and improve the overall performance of the forced dynamics (10). The ability to adapt the graph topologies in the forced dynamics is assumed to be restricted to the selection of a set of leader agents given at least $n_a \geq 2$ anchors. The topology selection problem is then a node selection rather than an edge selection problem.

With the objective of selecting a set of leader agents $S \subseteq V \setminus V_a$ to acquire the infinitesimally bearing rigid framework necessary for the convergence of the dynamics, the anchored rigidity matrix is

$$\mathcal{R}_a(S) = \begin{bmatrix} \mathcal{R} & \mathbf{0} \\ \frac{\partial \hat{\mathbf{g}}_a(S)}{\partial \mathbf{f}} & \mathbf{0} \end{bmatrix}$$

where $\hat{\mathbf{g}}_a(S) = \left\{\hat{\mathbf{f}}_{ij}\right\}$ where $i \in S$ and $j \in V_a$. Unlike the edge selection rigidity matrix problem, $2n_a$ rows are added to $\mathcal{R}_a$ for each leader selected. The matrix-valued set function $\widetilde{\mathcal{R}}_a(S)$ is defined similarly.

The following proposition establishes that the rank set function for $\mathcal{R}_a$ is submodular. Hence, the leader agents can be selected using greedy Alg. 1 until $\mathcal{R}_a$ has rank $2n$. Similar to the selection under rank in §4.1 the minimum number of leader agents, namely two will be selected.

Proposition 19. *The set function*

$$f_r(S) = \mathbf{rank}\left[\mathcal{R}_a(S)\right] \tag{28}$$

for $S \subseteq V \setminus V_a$ is submodular.

Proof: This result follows directly from Thm 13.a by letting $S_0 = \{1, 2, \ldots, 2m-1, 2m\}$ and

$$\begin{aligned} U(S) &= \mathcal{R}_a(S) \\ &= (I(S \cup S_0) \otimes I_{2n_a})\mathcal{R}_a(V \setminus V_a), \end{aligned}$$

where for $V \setminus V_a = \{v_1, v_2, \ldots, v_n\}$ then $\hat{\mathbf{g}}_a(V \setminus V_a) = \begin{bmatrix} \hat{\mathbf{g}}_a(\{v_1\})^T & \hat{\mathbf{g}}_a(\{v_2\})^T & \cdots & \hat{\mathbf{g}}_a(\{v_n\})^T \end{bmatrix}$. □

5.2 Leader Selection for Convergence

We now consider the selection of leaders under measures that promote the convergence rate of the dynamics. The matrix Q_a which appears in the Lyapunov function of Thm 18 can be written with respect to the leader set $S \subseteq V \setminus V_a$ as

$$Q_a(S) = \widetilde{\mathcal{R}}_a(S)^T \begin{bmatrix} \mathcal{D}_{\bar{k}}\left[m_{\bar{k}}^2 I_2\right] & 0 \\ 0 & \mathcal{D}_{\bar{k}_a(S)}\left[m_{\bar{k}}^2 I_2\right] \end{bmatrix} \widetilde{\mathcal{R}}_a(S), \tag{29}$$

where $\mathcal{D}_{\bar{k}}\left[m_{\bar{k}}^2 I_2\right]$ is constructed from the edges between agents in $V \setminus V_a$,

$$\mathcal{D}_{\bar{k}_a(S)}\left[m_{\bar{k}}^2 I_2\right] := (I(S) \otimes I_{2n_a})\,\mathcal{D}_{\bar{k}_a}\left[m_{\bar{k}}^2 I_2\right](I(S) \otimes I_{2n_a})^T,$$

and $\mathcal{D}_{\bar{k}_a}\left[m_{\bar{k}}^2 I_2\right]$ is constructed from the edges between the agent set $V \setminus V_a$ and the anchors V_a. Following a similar approach to §4.2, $\mathbf{trace}\left[Q_a(S)\right]$ is a modular function and the log of the determinant of a nullspace-removed $Q_a(S)$ is a submodular function with respect to the leader set S. This feature is summarized in the following two propositions. The proofs of these propositions are omitted due to their similarities to Props. 15 and 21.

Proposition 20. *Let $Q_a(S)$ be defined as in (29). The set function*

$$f_t(S) = \mathbf{trace}\left[Q_a(S)\right] \tag{30}$$

for $S \subseteq V \setminus V_a$ is modular.

Proposition 21. *Let $Q_a(S)$ be defined as in (29). The set function*

$$f_\ell(S) = \mathbf{logdet}[Q_a(S_R \cup S) + \begin{bmatrix} \mathbf{0}_{2n\times 2n} & \mathbf{0}_{2n\times 2n_s} \\ \mathbf{0}_{2n_s\times 2n} & I_{2n_a} \end{bmatrix}] \tag{31}$$

This article has been accepted for publication in a future issue of this journal, but has not been fully edited. Content may change prior to final publication. Citation information: DOI 10.1109/TNSE.2017.2754944, IEEE Transactions on Network Science and Engineering

where $S \subseteq V \backslash (V_a \cup S_R)$, and $\mathbf{rank}\left[f_\ell\left(\emptyset\right)\right] = \mathbf{rank}\left[Q_a(S_R)\right] = 2n$ *is submodular.*

As per §4.2, the greedy Alg. 1 can be applied to the set function (30) to select leaders that improve the convergence performance even when then the framework is not anchored infinitesimally bearing rigid. The logdet measure is applicable as a selection criteria once S_R leaders are selected which are sufficient to establish anchored infinitesimal bearing rigidity with $\mathbf{rank}\left[Q_a(S_R)\right] = 2n$. Additionally, positive linear combinations of the set functions (28), (30) and (31) are also submodular functions by Prop. 4. The suboptimality guarantees of Thm 5 would then apply to the greedy selection process. From the initial graph in Fig. 4d with four anchors present, Fig. 6a shows the selection of leaders under the measure $f_r\left(S\right) + \alpha f_t\left(S\right)$.

5.3 Edge Weight Selection

The edge weights $\mathbf{w}$ composed of the m initial edges and m_a anchored edges can be optimized similarly to §4.3. In the anchored case, the worst case convergence rate is dictated by the smallest nonzero eigenvalue of Q_a, namely $\lambda_{2n_a+1}(Q_a)$. Examining a reduced form of the anchored rigidity matrix defined as $\mathcal{R}_{ra} = \begin{bmatrix} \mathcal{R} \\ \frac{\partial \hat{\mathbf{g}}_a(S)}{\partial \mathbf{f}} \end{bmatrix}$, with the associated reduced unitless anchored rigidity matrix $\widetilde{\mathcal{R}}_{ra}$ then for $Q_{ra} := \widetilde{\mathcal{R}}_{ra}^T \mathcal{D}_{\bar{k}} \left[m_{\bar{k}}^2 I_2\right] \widetilde{\mathcal{R}}_{ra} \in \mathbb{R}^{2n \times 2n}$,

$$\lambda_{2n_a+1}(Q_a) = \lambda_1(Q_{ra}).$$

This follows from the removal of the nullspace of Q_a through the reduced anchored rigidity matrix. The dependence of Q_{ra} on $\mathbf{w}$ can be explicitly represented as $Q_{ra} = \sum_{s \in E} w_{\bar{s}} Q_{rau}(\{s\})$, where the matrix $Q_{au}(\{s\})$ represents the unweighted contribution of edge $s \in E$ to Q_{ra}. Subsequently, the maximization of $\lambda_{2n_a+1}(Q_a)$ can be represented as a linear matrix inequality (LMI) as shown in (32a).

The maximum control effort $u_{\max}$ of each agent in $V \setminus V_a$ can be distributed across the positive weights $\mathbf{w}$ through the inequalities (32b). It can often be desirable to explicitly encode the control effort limit devoted to the anchor edges $\mathbf{w}_a$ by the leader set V_ℓ. This flexibility can help avoid formation trajectories that are dominated by the anchor edges. In this direction, one approach is to upper bound the anchor edges weights contribution as $\sum_{j \in \mathcal{N}_a(i)} w_{ij} \leq \beta u_{\max}$ for $i \in V_\ell$ and $\beta \in (0, 1]$. To this end, denoting the submatrix of the incidence matrix corresponding to anchor edges as H_a then the anchor edge weight bound is equivalent to (32c). For $\beta = 1$, the anchor weight bound is inactive and anchor edges are constrained in the same fashion as the other edges in the network through inequalities (32b).

An attraction of the unforced dynamics (10b) is if small external signals are applied through $\tilde{\mathbf{u}}_i$ in (10a) then the formation transiently maintains its shape as it converges to a new translated and scaled formation [6]. A challenge with the external controls signal adopted in (27) is that the effect of the anchor edges can represent a large external signal that dramatically warps the formation shape. This can be mitigated though an edge weight design that limits the maximum control effort due to anchor edges. Inequality (32c) when β is close to 0 has this desired effect. The drawback from this approach is that it can induce a slower convergence to the desired formation. A demonstration of this is shown in Fig. 6b with the convergence of $\beta = 1$ much faster than that of $\beta = 0.1$. The trade-off is that for $\beta = 1$ then formation shape is largely distorted under scaling as indicated in the snapshots of the formation trajectory in Fig. 7a-c.

Algorithm 3 Convex optimization problem to maximize $\lambda_{2n_a+1}(Q_a)$ with respect to the weight vector $\mathbf{w}$ given a fixed edge set E.

$$\begin{aligned} \underset{\mathbf{w}}{\text{maximize}}\ & \delta \\ \text{s.t.}\ & \sum_{s \in E} w_{\bar{s}} Q_{rau}(\{s\}) \succeq \delta I, && \text{(32a)} \\ & \mathbf{w} \geq \mathbf{0},\ I(V \setminus V_a)^T \left|H^T\right| \mathbf{w} \leq u_{\max}\mathbf{1}, && \text{(32b)} \\ & I(V_\ell)^T \left|H_a^T\right| \mathbf{w}_a \leq \beta u_{\max}\mathbf{1} && \text{(32c)} \end{aligned}$$

An alternative, which is a marriage of fast convergence and small external signals in the face of a warped formation shape, is to replace the static weight w_{ij} on the anchor edges with a state-dependent edge weight $\overline{w}_{ij}$. The weight $\overline{w}_{ij}$ would ideally be small when the formation is "warped" and large otherwise. A local measure of the alignment of the formation is the error $\|\mathbf{u}_i\|$. A proposed *state dependent* anchor weight $\overline{w}_{ij}(\|\mathbf{u}_i\|)$ for $j \in \mathcal{N}_a(i)$ where $i \in V_\ell$ is

$$\bar{w}_{ij}(\|\mathbf{u}_i\|) = \frac{I(\{i\})^T \left|H^T\right| \mathbf{w} - \|\mathbf{u}_i\|}{I(\{i\})^T \left|H_a^T\right| \mathbf{w}_a} w_{ij}.$$

Here, $I(\{i\})^T \left|H^T\right| \mathbf{w}$ and $I(\{i\})^T \left|H_a^T\right| \mathbf{w}_a$ corresponds to the maximum available control effort available to agent i and to the anchor edges, respectively. As the formation becomes well aligned, $\|\mathbf{u}_i\|$ decreases and $\overline{w}_{ij}$ increases. Similarly, as the formation locally starts to warp the external signal supplied through the anchor edges is reduced. It should be noted that as $\|\mathbf{u}_i\| \leq I(\{i\})^T \left|H^T\right| \mathbf{w} - I(\{i\})^T \left|H_a^T\right| \mathbf{w}_a$ then $\overline{w}_{ij} \geq w_{ij}$. This positive weight is required for the convergence properties of Thm 18 to be applicable. Further, the maximum control effort of $u_{\max}$ is preserved in this case as

$$\begin{aligned} &\|\mathbf{u}_i + \tilde{\mathbf{u}}_i\| \leq \|\mathbf{u}_i\| + \|\tilde{\mathbf{u}}_i\| \text{ (from the triangle inequality)} \\ &\leq \sum_{j \in N(i)} w_{ij} + \sum_{j \in N_a(i)} \overline{w}_{ij}(\|\mathbf{u}_i\|) \text{ (as } \left\|(\hat{\mathbf{r}}_{ij}^T \hat{\mathbf{f}}_{ij}^\perp)\hat{\mathbf{r}}_{ij}^\perp\right\| \leq 1) \\ &\leq \sum_{j \in N(i)} w_{ij} + \sum_{j \in N_a(i)} \frac{I(\{i\})^T \left|H^T\right| \mathbf{w} - \|\mathbf{u}_i\|}{I(\{i\})^T \left|H_a^T\right| \mathbf{w}_a} w_{ij} \\ &= \|\mathbf{u}_i\| + \frac{I(\{i\})^T \left|H^T\right| \mathbf{w} - \|\mathbf{u}_i\|}{I(\{i\})^T \left|H_a^T\right| \mathbf{w}_a} \sum_{j \in N_a(i)} w_{ij} \\ &\leq \|\mathbf{u}_i\| + I(\{i\})^T \left|H^T\right| \mathbf{w} - \|\mathbf{u}_i\| \leq u_{\max}. \end{aligned}$$

Fig. 7 compares snapshots of the trajectories for the state-dependent solution with $\beta = 0.1$ to the non state-dependent dynamics with $\beta = 1$. Reduction to the distortion of the

This article has been accepted for publication in a future issue of this journal, but has not been fully edited. Content may change prior to final publication. Citation information: DOI 10.1109/TNSE.2017.2754944, IEEE Transactions on Network Science and Engineering

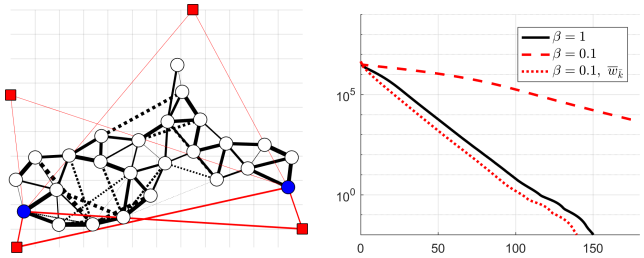

Figure 6: a) Weighted anchor selection using the function $f_r(S) + \alpha f_t(S)$ and b) convergence rates for aggressive anchor weights ($\beta = 1$), conservative anchor weights ($\beta = 0.1$) and state-dependent conservative anchor weights ($\beta = 0.1, \overline{w}_{\bar{k}}$). Anchor and leader nodes are represented by a filled square and circles, respectively.

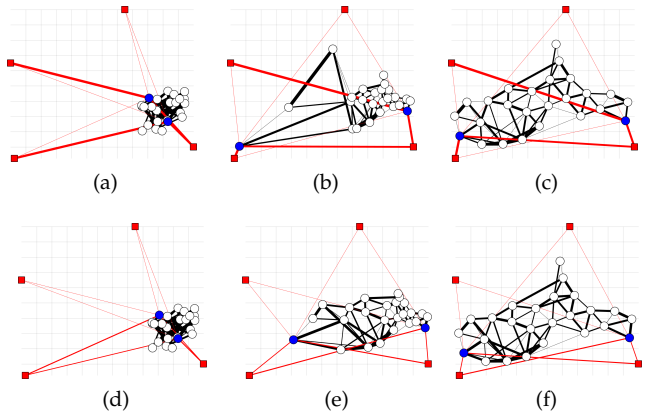

Figure 7: a-c) Trajectories for $\beta = 1$ and d-f) trajectories for $\beta = 0.1$ with state-dependent weighting. Anchor and leader nodes are represented by a filled square and circles, respectively

formation shape is noted and in addition the convergence rate in compared as shown in Fig. 6b.

6 Conclusion

In this paper, we built on our previous work on bearing-based dynamics for formation shape acquisition. The work examined connections between the graph topology and the performance of the dynamics. A bearing rigidity matrix weighted by the edge lengths on the underlying graph was shown to be critical in dictating stability and convergence of the resulting protocol. These connections allowed submodular optimization to be leveraged to select favorable edges based on guaranteeing bearing rigidity and promoting fast convergence. Further, the worst case convergence of the dynamics was examined in relation to the edge weights on the graph and a convex optimization framework was presented to select optimal edge weights.

An anchored version of the dynamics was also presented whereby a subset of the agents, called leaders, had access to bearing measurements to fixed landmarks. Anchored infinitesimally bearing rigidity was proven to be a necessary and sufficient condition for the convergence of the dynamics to a unique formation. The stability and convergence of the anchored dynamics was shown to be dependent on submodular set function on the selected leader agents, proving the greedy leader selection process exhibited close to optimal performance. A similar convex optimization problem to the unanchored case was presented to select optimal edge weights to improve the worst-case convergence of the anchored dynamics. With the motivation of preserving the formation shape in transients, a state-dependent weighted version of the anchored dynamics was proposed. In support of the dynamic weight selection, anchored bearing simulations demonstrated that the formation shape was more readily preserved compared to fixed edge weights.

The state-dependent weights on the anchor edges introduced in the final section of this work can be considered as a local memory-less feedback approach to preserve the formation scale. A direction of future work is to consider dynamic edge weights based on performance history. The objective would be to have a *learned* formation shape-preservation measure which would be used to inform the weight selection. On a more general front, the underlying machinery of the bearing dynamics is rigidity theory. A fruitful subject of future work would be developing a generalization of this theory with the goal of showing that efficient topology, leader, and weight selection can be attained based on submodular optimization and convex optimization for a large class of formation control problems.

References

[1] E. Schoof, A. Chapman, and M. Mesbahi, "Bearing-compass formation control: A human-swarm interaction perspective," in *American Control Conference*, 2014, pp. 3881–3886.

[2] R. Olfati-Saber and R. M. Murray, "Graph rigidity and distributed formation stabilization of multi-vehicle systems," in *IEEE Conference on Decision and Control*, 2002, pp. 2965–2971.

[3] N. Moshtagh, A. Jadbabaie, and K. Daniilidis, "Distributed coordination of dynamic rigid bodies," in *IEEE Conference on Decision and Control*, 2007, pp. 1480–1485.

[4] F. Dörfler and B. Francis, "Formation control of autonomous robots based on cooperative behavior," in *European Control Conference*, 2009, pp. 2432–2437.

[5] M. Basiri, A. N. Bishop, and P. Jensfelt, "Distributed Control of Triangular Formations with Angle-Only Constraints," *Systems & Control Letters*, vol. 59, no. 2, pp. 147–154, 2010.

[6] E. Schoof, A. Chapman, and M. Mesbahi, "Efficient leader selection for translation and scale of a bearing-compass formation," in *IEEE International Conference on Robotics and Automation*, 2015, pp. 1816–1821.

[7] F. Schiano, A. Franchi, D. Zelazo, and P. R. Giordano, "A rigidity-based decentralized bearing formation controller for groups of quadrotor UAVs," in *IEEE/RSJ International Conference on Intelligent Robots and Systems*, 2016, pp. 5099–5106.

[8] L. Krick, M. E. Broucke, and B. A. Francis, "Stabilization of infinitesimally rigid formations of multi-robot networks," in *IEEE Conference on Decision and Control*, 2008, pp. 477–482.

[9] M. Mesbahi and M. Egerstedt, *Graph Theoretic Methods in Multiagent Networks*. Princeton, New Jersey: Princeton University Press, 2010.

[10] N. Moshtagh, N. Michael, A. Jadbabaie, and K. Daniilidis, "Vision-Based, Distributed Control Laws for Motion Coordination of Nonholonomic Robots," *IEEE Transactions on Robotics*, vol. 25, no. 4, pp. 851–860, 2009.

[11] A. N. Bishop, I. Shames, and B. D. O. Anderson, "Stabilization of rigid formations with direction-only constraints," in *IEEE Conference on Decision and Control and European Control Conference*, 2011, pp. 746–752.

[12] A. Franchi and P. R. Giordano, "Decentralized control of parallel rigid formations with direction constraints and bearing measurements," in *IEEE Conference on Decision and Control*, 2012, pp. 5310–5317.

[13] S. Zhao and D. Zelazo, "Bearing Rigidity and Almost Global Bearing-Only Formation Stabilization," *IEEE Transactions on Automatic Control*, vol. 61, no. 5, pp. 1255–1268, 2016.

[14] Y. Wan, S. Roy, and A. Saberi, "Network design problems for controlling virus spread," in *IEEE Conference on Decision and Control*, 2007, pp. 3925–3932.

[15] A. Chapman and M. Mesbahi, "On strong structural controllability of networked dynamics: A constrained matching approach," in *Proc. American Control Conference*, 2013, pp. 6141–6146.

[16] D. Zelazo and M. Mesbahi, "Edge Agreement: Graph-Theoretic Performance Bounds and Passivity Analysis," *IEEE Transactions on Automatic Control*, vol. 56, no. 3, pp. 544–555, 2011.

[17] S. Boyd, "Convex optimization of graph Laplacian eigenvalues," *Proceedings of the International Congress of Mathematicians*, vol. 3, pp. 1311–1319, 2006.

[18] H. G. Tanner, G. J. Pappas, and V. Kumar, "Leader-to-Formation Stability," *IEEE Transactions on Robotics and Automation*, vol. 20, no. 3, pp. 443–455, jun 2004.

[19] D. V. Dimarogonas, P. Tsiotras, and K. J. Kyriakopoulos, "Leader-follower cooperative attitude control of multiple rigid bodies," *Systems and Control Letters*, vol. 58, no. 6, pp. 429–435, 2009.

[20] S. Zhao and D. Zelazo, "Localizability and distributed protocols for bearing-based network localization in arbitrary dimensions," *Automatica*, vol. 69, pp. 334–341, 2016.

[21] S. Patterson and B. Bamieh, "Leader selection for optimal network coherence," *IEEE Conference on Decision and Control*, pp. 2692–2697, 2010.

[22] A. Clark and R. Poovendran, "A submodular optimization framework for leader selection in linear multi-agent systems," in *IEEE Conference on Decision and Control*, 2011, pp. 3614–3621.

[23] F. Lin, M. Fardad, and M. R. Jovanović, "Algorithms for Leader Selection in Stochastically Forced Consensus Networks," *IEEE Transactions on Automatic Control*, vol. 59, no. 7, pp. 1789–1802, 2014.

[24] G. L. Nemhauser, L. A. Wolsey, and M. L. Fisher, "An Analysis of Approximations for Maximizing Submodular Set Functions I," *Mathematical Programming*, vol. 14, pp. 265–294, 1978.

[25] L. Lovász, "Submodular Functions and Convexity," in *Mathematical Programming The State of the Art*. Berlin: Springer, 1983, pp. 235–257.

[26] T. H. Summers, F. L. Cortesi, and J. Lygeros, "On Submodularity and Controllability in Complex Dynamical Networks," *IEEE Transactions on Control of Network Systems*, vol. 3, no. 1, pp. 91–101, 2016.

[27] A. Clark, B. Alomair, L. Bushnell, and R. Poovendran, *Submodularity in Dynamics and Control of Networked Systems*. Springer International Publishing, 2016.

[28] I. Shames and T. H. Summers, "Rigid Network Design via Submodular Set Function Optimization," *IEEE Transactions on Network Science and Engineering*, vol. 2, no. 3, pp. 84–96, 2015.

[29] H. K. Khalil, *Nonlinear Systems*. Prentice Hall, 2002.

[30] T. Eren, W. Whiteley, A. Morse, P. Belhumeur, and B. D. O. Anderson, "Sensor and network topologies of formations with direction, bearing, and angle information between agents," in *IEEE Conference on Decision and Control*, 2003, pp. 3064–3069.

[31] J. Cortés, S. Martínez, T. Karatas, F. Bullo, and S. Member, "Coverage Control for Mobile Sensing Networks," *IEEE Transactions on Robotics and Automation*, vol. 20, no. 2, pp. 243–255, 2004.

[32] K. R. Guruprasad and P. Dasgupta, "Distributed Voronoi partitioning for multi-robot systems with limited range sensors," in *IEEE International Conference on Intelligent Robots and Systems*, 2012, pp. 3546–3552.

[33] J. Stergiopoulos and A. Tzes, "Convex Voronoi space-partitioning for coverage purposes in heterogeneous sensor networks," in *European Control Conference*, 2009, pp. 2361–2366.

[34] H. H. Bauschke, O. Güler, A. S. Lewis, and H. S. Sendov, "Hyperbolic polynomials and convex analysis," *Canadian Journal of Mathematics*, vol. 53, no. 3, pp. 470–488, 2001.

[35] J. Khalife, K. Shamaei, and Z. M. Kassas, "A software-defined receiver architecture for cellular CDMA-based navigation," in *Position, Location and Navigation Symposium*, 2016, pp. 816–826.

Eric Schoof (S'12) received the B.S. degree in Applied and Computational Mathematical Sciences from the University of Washington, and the Ph.D. degree in Aeronautics and Astronautics at the University of Washington in 2017. He is currently a Research Fellow in the department of Electrical and Electronic Engineering at the University of Melbourne.

His research interests are networked dynamic systems and cooperative robotics with applications to multi-agent robotics and human-swarm interactions.

Airlie Chapman (M'14) received the B.S. degree in aeronautical engineering and the M.S. degree in engineering research from the University of Sydney, Australia, in 2006 and 2008, respectively, and the M.S. degree in mathematics and the Ph.D. degree in aeronautics and astronautics from the University of Washington, Seattle, in 2013. She is currently a Lecturer in the department of Mechanical Engineering at the University of Melbourne.

Her research interests are networked dynamic systems and graph theory with applications to multi-agent systems.

Mehran Mesbahi (F'15) received his Ph.D. degree from the University of Southern California, Los Angeles, in 1996. He was a member of the Guidance, Navigation, and Analysis Group at the Jet Propulsion Laboratory, California Institute of Technology, from 1996 to 2000 and an Assistant Professor of Aerospace Engineering and Mechanics, University of Minnesota from 2000 to 2002. He is currently a Professor of Aeronautics and Astronautics, Adjunct Professor of Mathematics, and Executive Director of the Joint Center for Aerospace Technology Innovation, at the University of Washington. His research interests are distributed and networked aerospace systems, systems and control theory, and engineering applications of optimization and combinatorics. Mehran Mesbahi is a Fellow of IEEE; he received the NSF CAREER Award in 2001, the NASA Space Act Award in 2004, the UW Distinguished Teaching Award in 2005, the UW College of Engineering Innovator Award in 2008, and the Graduate Instructor of the Year Award in 2015.